



LUND
UNIVERSITY

Master of Science dissertation:

In vivo knee cartilage quality assessment by direct quantification of glycosaminoglycans through chemical exchange saturation transfer (gagCEST)

Simon Kindvall

Supervisor:

Jonas Svensson

First submitted 2012-08-10

Returned 2012-09-11

Submitted again 2012-10-03

Department of Medical Radiation Physics, Malmö
Lund University, Sweden, 2012

Abstract

Introduction: Non-invasive imaging of human articular cartilage is an important tool in understanding, and thus allowing the development of effective treatments for, osteoarthritis; a disease responsible of impaired movement of millions of otherwise healthy individuals. Glycosaminoglycans (GAG) have been attributed with important biomechanical properties, vital for the function of the articular cartilage. By selectively irradiating hydroxyl protons at the GAG molecule and studying the saturation effect as it is transferred to water through chemical exchange, the GAG concentration can be inferred. This is termed glycosaminoglycan measurement through chemical exchange saturation transfer – gagCEST. This method would ideally directly measure the concentration of GAG in articular cartilage and increase the knowledge about osteoarthritis pathology. The aim of this thesis is to give the reader an understanding of the gagCEST method, and to evaluate a specific gagCEST work-in-progress (WIP) package.

Materials and methods: A WIP package for gagCEST measurements was evaluated on a Magnetom Trio 3 Tesla MRI system (Siemens AG, Erlangen, Germany), compatible with a 15 channel transmit/receive knee-coil. Phantoms with variable amount of GAG and agarose were measured in order to investigate the function of the system. Freeze dried samples of human femoral cartilage were supplied by the orthopedics department in order to optimize the measurement. Finally, several volunteers were scanned to test the *in vivo* applicability of the sequence at its current stage. Evaluation of measurements were done both using the raw data to create a CEST-spectrum in MatLab, as well as relying on the pixel-wise calculation of the CEST-image produced by the WIP programme.

Results: The gagCEST measurements proved to be filled with pitfalls. Phantom measurements were complicated by magnetic field inhomogeneity and incomplete gradient spoiling, grossly disturbing the CEST spectra. Though heterogeneity correction is applied, phantoms with lower T_2 relaxation must be produced to get rid of residual magnetization after spoiling. Despite this, some measurements were performed yielding a noticeable CEST effect when considering mean value of several pixels. *In vivo* measurements were first disturbed by fat chemical shift, but proved to produce images with CEST signal in cartilage. However, the evaluation of *in vivo* images was difficult, e.g., the CEST signal ratio between cartilage and meniscus was one order of magnitude away from the theoretically expected result.

Discussion: The gagCEST WIP sequence proved to provide image volumes in six minutes, displaying high signal in cartilage on healthy volunteers. However, the method requires additional extensive investigation. Phantom measurements are required to create standards and optimize the saturation sequence, for which low T_2 and long T_1 phantoms must be constructed. Moreover, *in vivo* measurements must be further scrutinized as magnetic field heterogeneity will quickly ruin a measurement; the cartilage of interest is tightly packed between bone and the meniscus. It is also important to realize that the gagCEST method does not in fact measure GAG, but rather labile hydroxyl protons, and there exist a possibility that other molecules will exhibit similar chemical shifts. Though this is not a physical but biochemical consideration it should be kept in mind when analyzing tissue and “gagCEST” signal. Finally, several authors claim the technique will be feasible at 7 T due to longer T_1 and larger chemical shift of GAG hydroxyls, however, it is evident from phantom tests that at least relative measurements are possible at 3 T.

Abbreviations

CEST	-	Chemical exchange saturation transfer
CS-A	-	Chondroitin sulfate-A
CW	-	Continuous wave (often saturation)
CWPE	-	Continuous wave power equivalent
dGEMRIC	-	Delayed gadolinium enhanced MRI of cartilage
ECM	-	Extracellular matrix
EPI	-	Echo planar imaging
FLASH	-	Fast low angle shot
GAG	-	Glycosaminoglycan
gagCEST	-	Glycosaminoglycan chemical exchange saturation transfer
MR	-	Magnetic resonance
MRI	-	Magnetic resonance imaging
MT	-	Magnetization transfer
MTC	-	Magnetization transfer contrast
NMR	-	Nuclear magnetic resonance
NOE	-	Nuclear Overhauser effect
OA	-	Osteoarthritis
PBS	-	Phosphate buffered saline solution
PSD	-	Power spectral density
pCMF	-	Posterior central medial femoral (region)
RF	-	Radio frequency
ROI	-	Region of interest
SAR	-	Specific absorption rate
WIP	-	Work in progress (regarding Siemens software)

Table of content

1	Introduction.....	5
1.1	Aim.....	5
2	Theoretical background.....	6
2.1.1	Diarthroidal joints.....	6
2.1.2	Articular cartilage	7
2.1.3	Chondroitin sulfate.....	8
2.1.4	Osteoarthritis	9
2.2	Physics of CEST	10
2.2.1	Magnetization transfer - theoretical background	10
2.2.2	Chemical exchange	10
2.2.3	CEST imaging introduction	12
2.2.4	CEST spectrum.....	13
2.2.5	Inhomogeneity correction.....	14
2.2.6	Saturation pulses.....	14
2.2.7	gagCEST	17
2.2.8	Current state of gagCEST imaging	17
3	Methods	18
3.1	MRI Hardware	18
3.2	MRI pulse sequence and CEST image calculation	18
3.3	Measurements	20
3.3.1	Chondroitin sulfate and PBS phantoms.....	20
3.3.2	Low T ₂ measurement with CS-A and DOTAREM.....	21
3.3.3	Chondroitin sulfate and agarose gel phantoms	21
3.3.4	Cartilage samples	22
3.3.5	<i>In vivo</i> measurement with healthy volunteers.....	22
3.4	MR imaging parameters	23
3.5	Data processing	23
3.5.1	Chondroitin sulfate and PBS phantoms.....	23
3.5.2	Low T ₂ measurement with CS-A and DOTAREM.....	24
3.5.3	Chondroitin sulfate and agarose gel phantoms	24
3.5.4	Cartilage samples	24
3.5.5	<i>In vivo</i> measurement with healthy volunteers.....	24
4	Results	25

4.1	Chondroitin sulfate and PBS phantoms.....	25
4.2	Low T_2 measurement with CS-A and DOTAREM.....	28
4.3	Chondroitin sulfate and agarose gel phantoms	29
4.4	Cartilage sample measurements.....	32
4.5	<i>In vivo</i> measurement with healthy volunteers.....	34
5	Discussion	41
5.1	Discussion of results	41
5.1.1	Chondroitin sulfate and PBS phantoms.....	41
5.1.2	Low T_2 measurement with CS-A and DOTAREM.....	42
5.1.3	Chondroitin sulfate and agarose gel phantoms	42
5.1.4	Cartilage samples	42
5.1.5	<i>In vivo</i> measurement with healthy volunteers.....	43
5.2	Clinical future	44
5.3	Improvements and further studies	44
6	References.....	45
7	Appendix.....	48
7.1	Investigation of ring artefacts in CEST-measurements	48

About this paper

This report is the written part of a Master thesis project for examination as a master of science in medical physics at Lund University done over the spring semester of 2012. The work was done at Skånes universitetssjukhus (SUS) in Malmö at the Medical radiation Physics department with Jonas Svensson as supervisor. Furthermore, it is written to mirror the effort put into investigating the gagCEST-effect and the trials associated with the work. It is meant to be read by peers in order to better understand the CEST and particularly gagCEST-applications since not much work has been done in this area in Scandinavia. Thus, it is written explicitly to medical physicists or other professionals/researchers with knowledge of basic magnetic resonance theory but it requires no previous familiarity with clinical CEST-applications or cartilage imaging in general.

1 Introduction

Osteoarthritis (OA) is one of the major non-lethal health issues of the modern world, whose cost has been approximated to 1 % of the gross domestic product of developing countries [1]. This has led to large efforts to understand and quantify the disease in clinical settings. It is now well understood that late OA is associated with degradation and decrease in size of important cartilage protein complexes, aggrecans, with glycosaminoglycan (GAG) being its main constituent [1]. Delayed gadolinium enhanced MRI of cartilage (dGEMRIC) is a method devised to measure the quality of cartilage with respect to its GAG content. Several studies have successfully illustrated the correlation between dGEMRIC-index and OA[2]. However, the method is based on the injection of MRI contrast agent and subsequent diffusion of contrast into the synovial cavity and cartilage and is thus an indirect method for cartilage GAG measurement. This, together with time consuming routines limits the applicability of the method to some extent. Ling et al. suggested glycosaminoglycan assessment by chemical exchange saturation transfer (gagCEST) as a completely noninvasive alternative, able to directly measure the content of GAG by selectively saturating labile protons on the GAG molecule and study the effect as magnetization is transferred to bulk water [3]. In opposition, Singh et al. convincingly suggested that the results of the previous group originated in the lack of B_1 correction and thus questioned the feasibility of the method at 3 Tesla. Other groups have used gagCEST to evaluate novel cartilage repair techniques in junction with sodium imaging [4], as well as investigating the GAG content of intervertebral discs [5]. The problem is that no one has outlined the actual relationship between gagCEST image signal and the GAG content *in vivo*, which inhibits the initiation of gagCEST measurements as a clinical routine. This in turn is a consequence of the fact that the method has not yet been optimized and standardized.

The scope of this work was intended as a pilot study of the gagCEST MRI sequence, including phantom experiments with various amounts of GAG; *in vitro* cartilage imaging and quality assessment; and a limited number of *in vivo* cartilage images to test the clinical applicability.

The report contains images and results from all three series of investigations as well as a thorough description of the gagCEST technique as portrayed in the literature. The feasibility of clinical gagCEST at 3 T is still questionable – specifically due to the high sensitivity to field inhomogeneities, however, other applications of CEST does exist, including agents with other saturation targets which are less sensitive to inhomogeneity and other macroscopic parameters.

1.1 Aim

The aim of the master thesis was explicitly to gain understanding of the gagCEST-technique and assess the clinical applicability for cartilage GAG content measurements at 3 T magnetic field strength. To narrow the investigation the focus has been on the Siemens Trio 3T system and a work in progress (WIP) sequence, delivered as part of a research collaboration between SUS-Malmö and

Siemens. Since clinical application of gagCEST is relatively novel and no trials has been conducted in Sweden the first priority was simply to understand and describe the phenomenon in detail. Secondly, it was desirable to investigate whether the technique was at all clinically applicable. This was done in three steps; by phantom experiments with the purpose of creating a standard gagCEST reference phantom where the CEST image pixel amplitude ideally would correlate with GAG concentration; an *in vitro* study of knee cartilage where visibly pathologic and fresh cartilage could be imaged; finally, healthy subjects were imaged to optimize imaging parameters *in vivo*. In light of the results from these investigations, further experiments and clinical trials can be designed.

2 Theoretical background

2.1.1 Diarthroidal joints

The knee is a diarthroidal joint, chosen as the subject of this study for mainly two reasons; first, the knee is one of the most stressed joints with cartilage high in GAG content, secondly, the knee is easy to study in the MRI-scanner. Joints can be categorized according to the range of motion where diarthroidal joints – also referred to as diarthrosis or synovial joints – represent the most flexible type, responsible for nearly frictionless motion throughout a lifetime as well as absorbing shocks of several times the weight of the body during various exercises. The joint is enclosed in a synovial capsule containing synovial fluid for maximum lubrication and it is possible to analyze this fluid for residual proteins in order to diagnose diseased joints. However, the penetration of the synovial membrane is coupled with a risk of infection, which makes all non-invasive methods for joint investigation interesting. Furthermore, most diagnostic centers have specific knee-coils giving high SNR and low SAR due to local RF-transmission and reception, the former being imperative for high SAR pulse sequences, thereby allowing specialized studies in this anatomic region.

Excellent public domain anatomical depictions of the knee joint are found in Gray's Anatomy from 1918 as shown in Figure 2-1. Here the articulating surfaces of the femoral condyles are visible along with the menisci and ligaments.

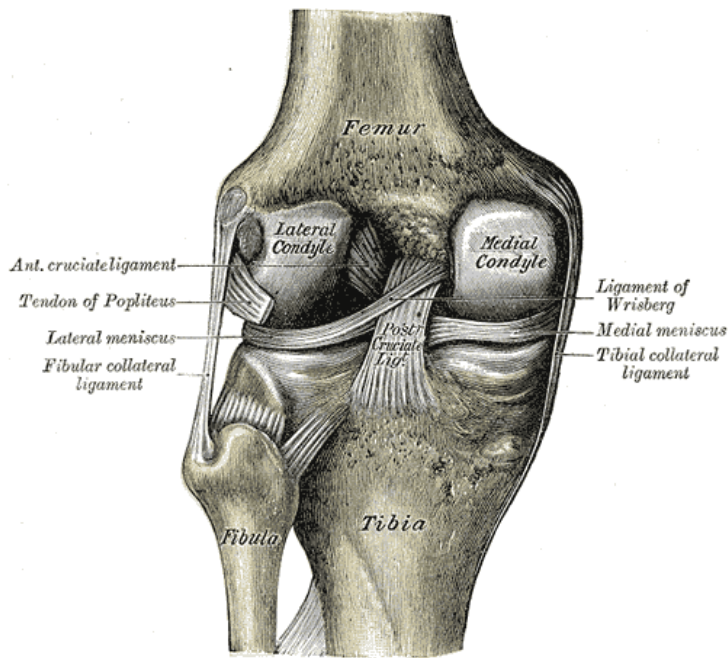


Figure 2-1 Posterior view of left knee joint. (H Gray, *Anatomy of the human body*, 1918)

2.1.2 Articular cartilage

Joint lubrication and shock absorption is ideally accomplished by hyaline cartilage; a hypoxic tissue only a few millimeters thick with a rigid and shock resistant extra cellular matrix (ECM) containing neither blood vessels nor nerves. The overall composition of the articular cartilage is described in Table 2-1 where collagen fibers and the proteoglycan aggrecan can be seen to be abundant. The shock absorbing properties of the tissue comes from the interaction of these two molecules, where the aggrecan pressure is opposed by the tensile strength of collagen as illustrated in Figure 2-2 [6]. Ideally this tissue configuration will function throughout a lifetime, supported only by slow turnover of the molecules [7]. However, disruption of the synthesis and degradation will result in pathology [8].

Table 2-1 Hyaline cartilage composition according to Dudhia and Torshizy, Gold and Chung.

Component	Approximate wet weight [%]	
	Dudhia [7]	Torshizy, Gold, Chung [9]
Water	70	60 – 80
Type II Collagen	18	12 – 24
Proteoglycan		6 – 12
Aggrecan	5	
Chondrocytes		5

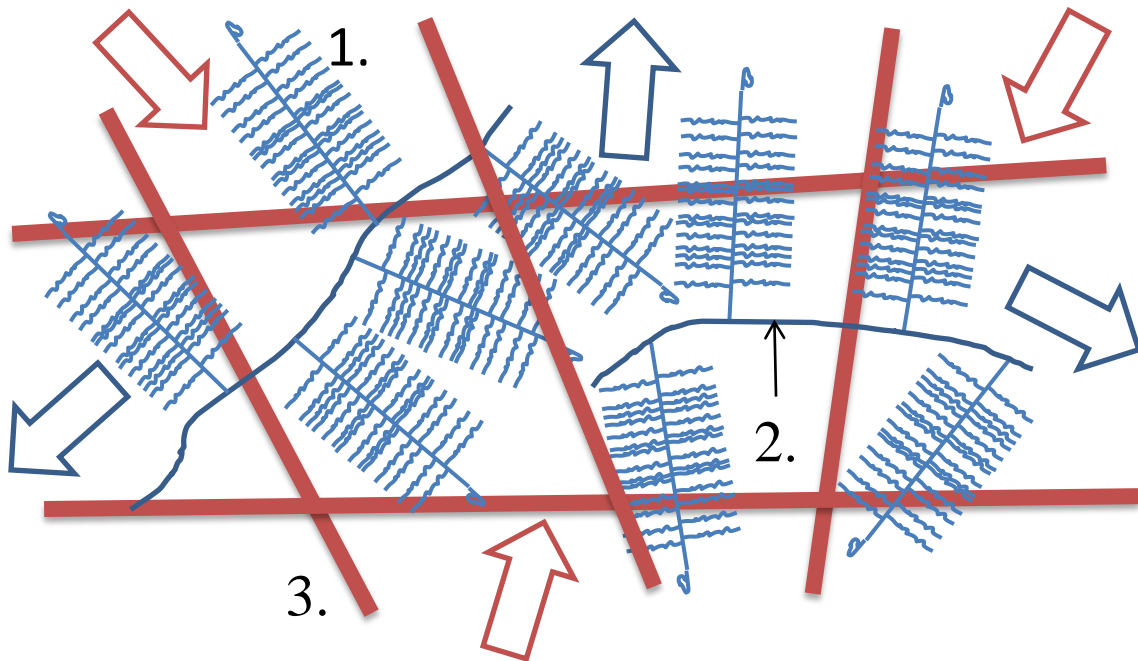


Figure 2-2 Schematic drawing of articular cartilage ECM: (1) large aggrecan molecule bound to (2) hyaluronan chain, creating an osmotic pressure (blue arrow) against (3) the rigid collagen fibril network.

The aggregate consist of a central stem of the glycosaminoglycan (GAG) hyaluronan (HA) onto which hundreds of aggrecan and link-protein molecules are attached giving rise to structures weighing a total of 10^8 - 10^9 u [7]. The aggrecan in turn is made of a core protein upon which functional groups have been substituted with GAG chains of the types chondroitin sulphate and keratan sulphate (CS and KS) where the CS chains are three times more common than KS in numbers [7], but also twice as heavy (20 000 u compared to 10 000 u [7, 6]) . Since the core protein constitutes approximately 10-20 % of the molecular weight of aggrecan [7, 6], it is reasonable to assume a CS concentration of approximately 4 % by mass in healthy articular cartilage.

2.1.3 Chondroitin sulfate

The primary glycosaminoglycans of interest in this context are the isomers of chondroitin sulfate (CS) referred to as CS-A and CS-D which differ in the position of the sulfate group. The polymers consist of disaccharide units of N-Acetylgalactoseamine (molecular weight 221.21 g/mol) and glucuronic acid (molecular weight 194.14 g/mol) as shown in Figure 2-3

The polyanionic chains of CS repel each other electrostatically giving the aggrecan molecule its typical “broom shape” which ensure they occupy the maximum possible space in the ECM. Furthermore, the charge will readily attract sodium ions, creating an additional osmotic water pressure. These processes are largely considered the biomechanical mechanism for the stiffness and resistance of articular cartilage[6, 7, 9].

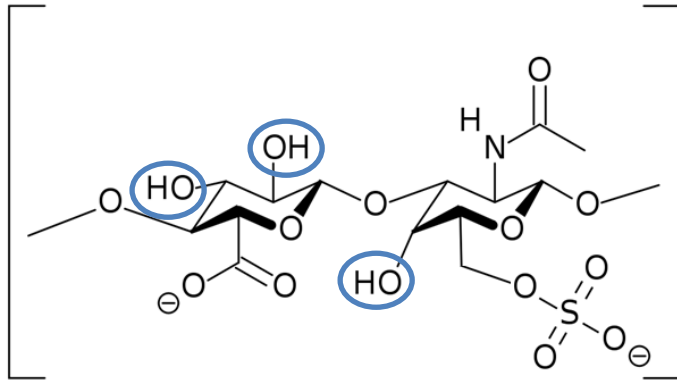


Figure 2-3 Chondroitin-6-sulphate or CS-C disaccharide unit. This isomer differs in placement of the sulphate group compared to the CS-A type. Labile hydroxyl groups are circled due to their importance in the gagCEST application (see section 2.2.3.)

2.1.4 Osteoarthritis

Osteoarthritis (OA) is characterized by loss and degradation of articular cartilage. The disease is initiated at the joint surface where the tissue is most stressed and spreads throughout the matrix until reaching the subchondral bone. The process can induce local inflammation, possibly synovitis (inflammation of the synovial membrane) and pain [10, 1]. Histological features in late OA include the fibrillation of tissue, patchy loss of aggrecan and clustering of chondrocytes, rendering a largely more inhomogeneous tissue [8, 1].

Despite being widespread and causing much pain and loss of productivity, no medical cure for OA has yet been put in clinical use. Patients are rather prescribed different disease management and methods, including weight loss and training, as well as being offered support tools and physiotherapy. Prophylactic works is also important, for example, patients with meniscal injury has shown a 50 % incidence of OA in ten years [1], whereas training and dynamic loading, where pressure is relieved by muscular strength, decreases the risk of OA [10]. Inflammatory responses to late disease are treated symptomatically and for progressed OA, joint replacement with prosthesis is common.

The biomechanical background for the disease has been investigated and the consensus is that the disease is associated with a decrease in size of the aggrecan molecule as well as an overall decrease of its concentration in the ECM [7], motivating a direct method to measure the concentration of GAG. In a recent report, however, Stubendorff et al. concluded that GAG content was not a specific marker for early OA, as opposed to water content which increased in early stages of the disease [8]. These findings in light of the previously mentioned theory for OA pathogenesis, makes a direct method for in vivo GAG content measurement of paramount interest in order to understand the disease [8]; does OA trigger a decrease in aggrecan size and concentration or does aggrecan degradation trigger OA? Since the disease is developed under many years, preclinical data is vary sparse and non-invasive method for cartilage quality assessment is a first step in tracking the early changes leading to pathology.

2.2 Physics of CEST

2.2.1 Magnetization transfer - theoretical background

Magnetization transfer (MT) is a straightforward term describing the transfer of longitudinal magnetization from one environment to another. This can occur by dipolar cross relaxation through space or by direct exchange of protons from one environment to another. Considering two spins I and S, represented by blue and white circles in Figure 2-4, the relaxation of S is most likely to occur if it is perturbed by I, as indicated by the blue arrows in the figure. However, relaxation of S can also occur by the excitation of the I-spin as indicated with the horizontal black arrow, termed W_0 , in the figure [11]; or by the stimulated relaxation of both spins indicated by the vertical black arrow which is called the W_2 pathway [12]. The latter magnetization transfer pathway is referred to as the nuclear Overhauser effect (NOE) and is a purely quantum mechanical and nuclear phenomenon between bound nuclei close to each other in space. For large rigid molecules the likelihood for the W_0 cross relaxation pathway is dominating, since it is associated with zero or a small total energy difference $hf_1 - hf_2$. The stimulated relaxation pathway is more common in small, quickly tumbling molecules since it is associated with a large energy difference $hf_1 + hf_2$. The MT effect has been utilized for magnetization transfer contrast imaging (MTC) in tissue where water is bound to macromolecules [11]. Generally, the correlation times of macromolecular structures are so long that T_2 is in the order of 10 μ s, making them impossible candidates for direct imaging. However, the short T_2 means the absorption spectra are in the order of several kHz. Pulses applied at frequencies far from the water resonance will thus affect the macromolecules, through which the magnetization is transferred to nearby water protons. For example, this has been utilized for MT suppression of soft tissue to improve image quality in MR angiography [13].

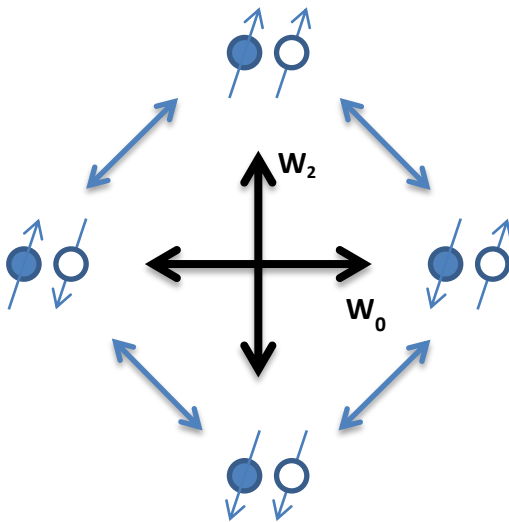


Figure 2-4 Illustration of dipolar coupling pathways between two protons close in space. Cross relaxation in a two spin system can occur in six ways. NOE is indicated by black arrows

2.2.2 Chemical exchange

Chemical exchange (CE) is very similar to the W_0 cross-relaxation and is the major MT pathway in systems where atoms are loosely bound such as amide groups or hydroxyls. These protons tend to make spontaneous inter- or intramolecular exchange – leading to a change in magnetic environment of the individual spins, but not to a chemical reaction. The phenomenon has long been a tool in

understanding the configuration of complex compounds, catalyst action and pH monitoring in NMR. CE may also refer to a rotating functional group, or a delocalized pi-bond, where the magnetic environment of a single spin changes, without changing the chemical properties of the molecule, but this type of CE is not interesting in CEST applications.

A very thorough explanation of CE, including Bloch-equations, is given by Bain in a review [14]. A brief mathematical description is given for the curious reader. By defining a complex magnetization in the xy -plane as $M = u + iv$ and defining the magnetization of two atoms in different chemical environments as M_A and M_B the magnetization at the end of an excitation pulse is described by the equation below:

$$\frac{d}{dt} \begin{pmatrix} M_A \\ M_B \end{pmatrix} = -L \begin{pmatrix} M_A \\ M_B \end{pmatrix} \quad \text{Eq. 2.1}$$

Solutions to this equation are exponentials. The matrix L contains the chemical shift difference, δ , between the environments A and B; the transversal relaxation of the system T_2 ; as well as the exchange governed by the rate constant k . Solving for the eigenvalues of the matrix yields an expression containing the term $\sqrt{k^2 - \delta^2}$. When the rate of exchange is larger than the chemical shift, this term is positive. This means that there is no complex (oscillating) term in the exponential solution and the NMR spectrum will show a single peak. At lower rates there will be a complex component of the eigenvalue (oscillating term) giving rise to two lines in the NMR spectrum. This is the classic CE-effect utilized in NMR spectroscopy and has little to do with the CEST-method. However, the terms fast and slow exchange does recur in CEST applications and refers to the rate constant being large or small compared to the chemical shift difference between the pools. It should be noted that pH and temperature has a direct effect on the rate constants of chemical exchange, making them important controlled variables in any CEST experiment, however, physiological temperature and pH is often favorable.

One important feature of nuclei participating in chemical exchange is the difficulty to perform MR-spectrometric analysis on them. During slow exchange the signal from each type of nucleus will be visible as a peak in the FID-spectrum, given by δ in the limit of small k (a complex component of the Bloch equation eigenvalue gives an oscillating term). As the exchange rate increases – for example through increased temperature or pH – the peaks will broaden unsymmetrically, coalesce and finally disappear until they reappear at the population mean as illustrated in Figure 2-5. The whole process can occur during a limited temperature range, eg., going from 270 to 300 K. This implies that there will be no visible peak in the NMR spectrum for a functional group proton in fast chemical exchange with water, since the water protons are always more abundant.

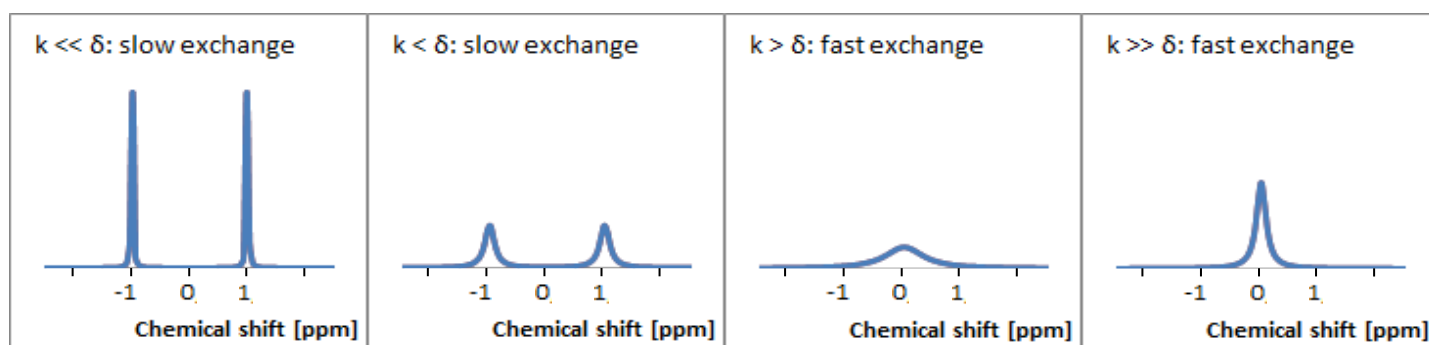


Figure 2-5 Simplified illustration of NMR spectrum during two pool chemical exchange going from slow to fast exchange rate. The chemical shift between the pools is assumed to be 2 ppm and phase asymmetry is ignored.

2.2.3 CEST imaging introduction

The idea to image the chemical exchange effects were presented by several authors including Balaban [15] and McFarland [16] in 1988 and 1990. The basic concept is unchanged and only requires a solute with a labile proton, chemically shifted a few ppm from the water resonance. Solute protons which are irradiated at their resonant frequency will be selectively saturated, the subsequent chemical exchange will transfer these protons to the surrounding water, and the water signal will decrease as illustrated in Figure 2-6. If the T_1 relaxation time of the solvent is sufficiently long for the saturation effect to persist, subsequent measurement will show a decrease in signal in the bulk water population due to saturation transfer, and the signal loss will depend directly on the concentration of the functional group initially saturated.

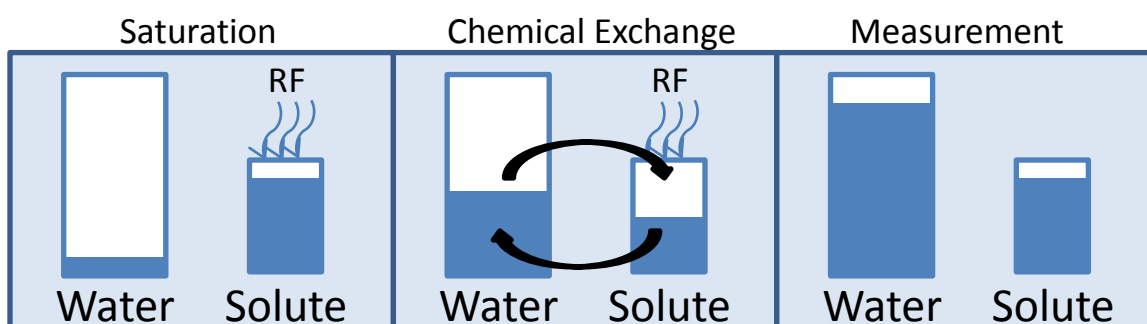


Figure 2-6 Illustration of the CEST effect, rectangles represent magnetization at equilibrium, shaded area represent saturated spins. Selective saturation at a solute resonance will be transferred to the water pool through chemical exchange. In practice, saturation and exchange occur almost simultaneously. If saturation is applied long enough ($T_{\text{sat}} = \text{seconds}$) the subsequent measurement of MR signal will reveal a decrease in water signal due to the transferred saturation effect.

CEST measurements are mostly performed in two steps with a saturation period and a read-out period as illustrated in Figure 2-7, where the latter can be almost any conventional pulse sequence. For NMR experiments with CEST it is enough with a single saturation pulse, however, in case of imaging the sequence must be segmented unless extremely fast techniques, such as echo planar imaging (EPI) is utilized, since the measurement must be completed before the saturation effect wears off. The chemical exchange occurs at rates between 10 – 1000 Hz, and saturation is active during 100 – 1000 ms, implying a continuous transfer of saturation effect to the bulk water during the saturation period. This is followed by the collection of one or more k-space lines before a new saturation period begins, since saturation effect is lost by longitudinal relaxation.

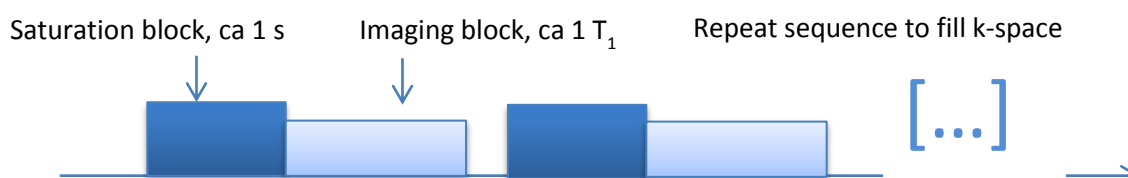


Figure 2-7 Illustration of CEST imaging sequence, saturation effect is lost with longitudinal relaxation so saturation pulses and imaging must be interleaved to achieve CEST contrast.

In Balaban's initial experiment ammonia was used as CEST agent in water which gives a chemical shift difference, δ , of 2.5 ppm. He stated in a paper that this could amplify the detectability of the solute

1000-fold under optimal conditions [15] but the technique was most successful as a means of determining the rate constant of the chemical exchange. In the same article Balaban produced a simple CEST image. This was done by acquiring two images; one with saturation preparation at the ammonia resonance, 2.5 ppm higher than the water resonance and one control image with saturation prepulse at 2.5 ppm lower than the water resonance. The ratio of these images gives a measure of the CEST effect. Balaban stated that *in vivo* CEST imaging would be complicated by the macromolecular MT effects as outlined earlier, but with “proper control irradiation” these problems would be mitigated [15]. The collection of a CEST spectrum is a way to do this.

2.2.4 CEST spectrum

Considering an ideal CE system with a small solute pool, such as glycosaminoglycan, in a large solvent pool like water, the NMR spectrum would look somewhat like the upper part of the graph in Figure 2-8. As a saturation pulse is applied far away from the water proton Larmor frequency, a small decrease in water signal will be visible due to the finite bandwidth of the saturation pulse and the symmetric magnetization transfer in the medium – collectively referred to as spillover. The most substantial effect is naturally when the saturation pulse is at the water resonance. This will lead to a drastic decrease in the MR signal. However, what is interesting is a pulse applied at the resonance frequency of a solute proton exhibiting chemical exchange, here the solute will be saturated and the CE will transfer the saturation effect to the solvent, leading to a substantial reduction in the MR signal. The lower part of Figure 2-8 depicts this; a plot of the signal intensity as a function of the saturation pulse frequency is termed a Z-spectrum in classical magnetization transfer experiments. However, as it is utilized in the study of CEST phenomena it is also called a CEST-spectrum.

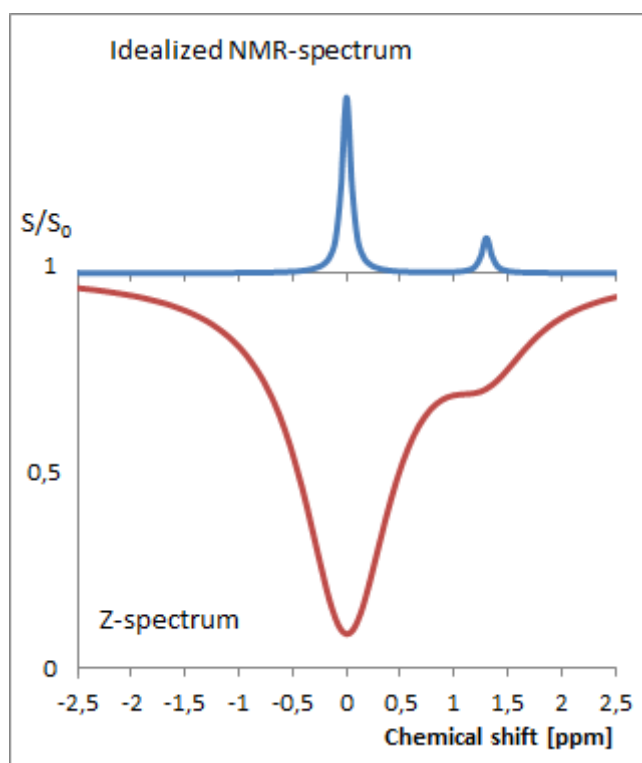


Figure 2-8 Combination of ideal NMR-spectrum (blue line, top) with Z-spectrum (red line, bottom), during slow exchange, showing the intensity variation of the MR signal as saturation pulses are applied at different chemical shifts, referred to as CEST-spectrum if CE is the MT pathway studied.

2.2.5 Inhomogeneity correction

Since CEST induces a decrease in signal intensity, a subtraction of two images is the most simple case of creating a positive CEST contrast; one image with a selective saturation pulse on the CEST-agent resonance and one with saturation on the opposite side of the bulk water resonance. This, however, requires the exact resonance frequency of the water pool to be well known, which in practice means a completely homogeneous B_0 field. Since this is seldom the case in clinical imaging or phantom measurements in general, correction of inhomogeneity has been an issue in the context of CEST. The effect of an inhomogeneous B_0 field is straightforward, considering the Z-spectrum: a shift in frequency will make the curve more asymmetric and either completely remove the visibility of the CEST effect, or grossly amplify it [17]. However, instead of spending endless efforts on field shimming and create a perfectly homogeneous B_0 field, most methods are oriented about finding the water resonance in each pixel or voxel during imaging. Water shift saturation referencing, abbreviated WASSR, is such an example where low power saturation pulses are applied at several chemical shifts, and the signal minima will represent the true water frequency [18]. The idea is to only look at a narrow spectrum of direct water saturation with little or no MT effects, the CEST spectrum can accordingly be shifted to eliminate false asymmetry as illustrated in Figure 2-9.

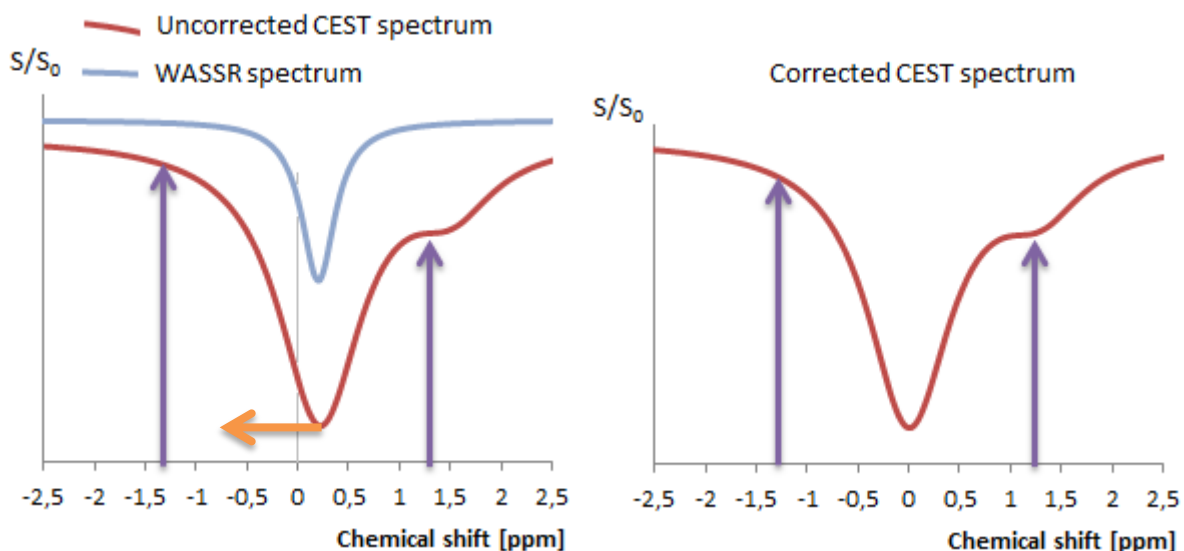


Figure 2-9 Illustration of water shift saturation referencing, WASSR, as a method to correct for B_0 inhomogeneity. Comparison of the signal at the CEST agent chemical shift and control side must be symmetric about the water frequency (indicated by purple arrows). The narrow blue WASSR spectrum identifies the water resonance in each pixel and allows correction of the CEST spectrum (orange arrow).

2.2.6 Saturation pulses

The saturation pulse is of primary interest in CEST imaging. Originally continuous wave (CW) excitation was used but due to hardware and SAR constraints, most applications are now employing a pulsed saturation technique [19]. To understand CW saturation it can be considered as longitudinal spoiling – the magnetization vector is rotated around the x-axis until the phase coherence inside a voxel is lost, resulting in a net magnetization of zero in all directions. Another interpretation is that spins are pumped with more energy than can be dissipated and thus become randomized due to a shift of the thermal equilibrium given by the Boltzmann distribution. The point of pulsed saturation is to achieve the same saturation effect but with reduced SAR and RF output. This is commonly done by

one or more excitation pulses together with transversal spoiler gradients. In such saturation schemes, however, there is a risk of residual magnetization which accidentally is recovered by subsequent excitations and spoiler gradients.

The main saturation parameter of interest in the CEST application is the total saturation time, t_{sat} , before the imaging segment. The rate of change of saturation depends on the chemical exchange rate and apparent longitudinal relaxation, giving a differential equation, simplified and solved by Zhou et al. into the following form [20].

$$CEST \propto \frac{k_{ws}}{R_{1w} + k_{ws}} (1 - \exp(-r_{1w} \cdot t_{sat}))$$

Here k_{ws} is the chemical exchange rate, R_{1w} is the longitudinal relaxation rate of the pool (water) and r_{1w} is the apparent relaxation rate during irradiation. As can be seen in Figure 2-10, optimal saturation efficiency is achieved after several T_1 – though Schmitt et al. reported no significant increase in CEST effect after $2 \cdot T_1$ [21]. However, maximum saturation per time is achieved for short saturation times, which is preferable since scan times in MRI imaging is already rather long. For solutes with slow exchange rate, however, it is possible to flip the magnetization vector 360° with long saturation pulses, the CEST effect as a function of saturation time will then display a sinusoidal response [19].

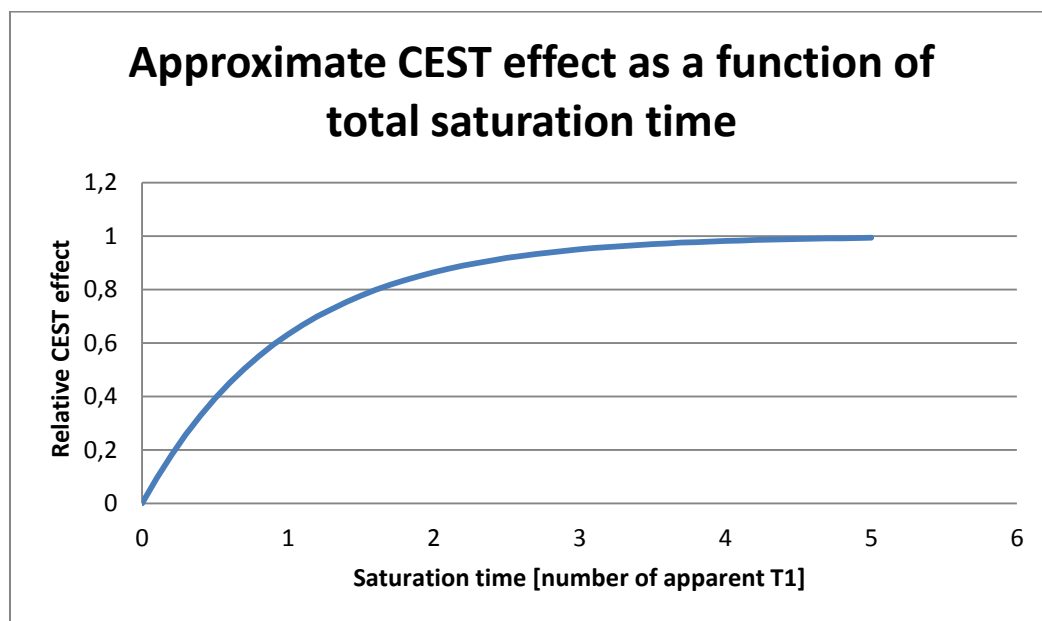


Figure 2-10 Illustration of relative CEST effect as function of total saturation time t_s . The time scale is in numbers of apparent T_1 . The actual slope of the curve also depends on CE-rate.

Next to saturation time, the saturation power is the main parameter determining the saturation efficiency. This is often measured in continuous wave power equivalent - CWPE. Sun et al. and Zu et al. have studied the CEST effect as a function of CWPE, the former at 4.7 T and the latter at 9 T [19, 22]. Both agree that there is an optimal CWPE amplitude for a given CEST molecule. As saturation power is increased more saturation effect is transferred to the liquid pool and CEST effect is increased until reaching a fairly stable value. This occurs when the saturation frequency, $B_1\gamma = \omega$, is close to the chemical exchange rate k_{sw} . However, the effect does not increase beyond this point due to more prominent spillover effects which gives rise to direct saturation – masking the CEST effect. Analytical approximations describing the behavior before and after this plateau have been

presented by Sun et al. [22], and are referred to as the weak and strong saturation pulse approximation, respectively. Zu et al. performed similar simulations for the pulsed CEST-experiment and also found a plateau for maximum CEST-effect which correspond to the CW-case. Though the position of the plateau differs with solute chemical shift, duty cycle of the saturation pulses, chemical exchange rate and saturation flip angle, imaging should be possible and insensitive to B_1 heterogeneity once this plateau is found [23].

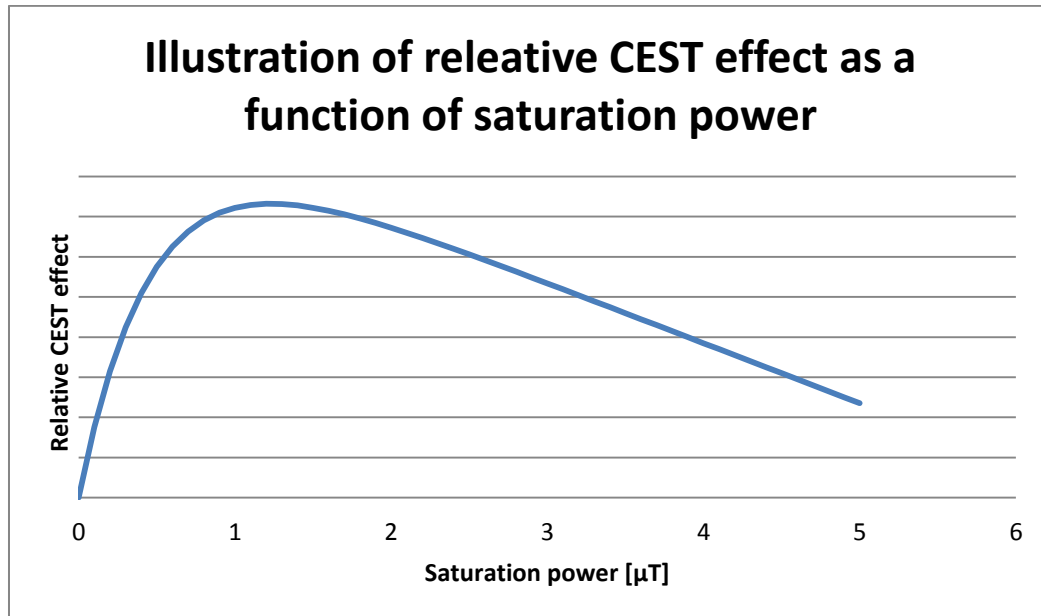


Figure 2-11 Schematic illustration of CEST effect as function of saturation power for arbitrary CEST-agent. The CEST effect reaches a maximum as the saturation frequency approaches the chemical exchange rate, at higher power direct spillover effects dominate.

Finally, in order to optimize the measurement of CEST agents the spectral content of the saturation pulse train must be known. The calculation is not trivial; the power spectral density (PSD) function width of a saturation pulse is in the same order of magnitude as the chemical shift of the CEST agent. This is quickly realized as $\Delta f \propto 1/\Delta t$ making the pulse time of 10-100 ms corresponding to a frequency distribution in the order of 10 – 100 Hz. A Gaussian pulse is described by the following equation:

$$B_1(t) = \frac{A}{\sqrt{2\pi} \cdot \sigma} \exp\left(\frac{-(t - t_0)^2}{2\sigma^2}\right)$$

In the equation, σ is the major parameter determining spillover and is related to the pulse length. If the pulse length and interpulse delay are identical, >99% RF energy will be deposited within $3/\sigma$ at each side of the center frequency, and generally $BW \approx 6/\tau_p$ where τ_p is the pulse duration [21]. For a 100 ms pulse this is 0.47 ppm, and for 33 ms this is 1.42 ppm. These values are only approximate, since the excitation pulses are truncated, moreover, in the present investigation the pulse duration and interpulse delay are different. The PSD of three 99 ms Gaussian pulses with 9 ms interpulse delay is calculated in MatLab and shows that virtually no RF power will be deposited beyond 20 Hz of the center frequency, giving an effective bandwidth of 0.3 ppm, as illustrated in Figure 2-12. This discussion has not included the effects of spoiler gradients which makes the calculation even more complicated – and nonetheless more interesting for further investigation.

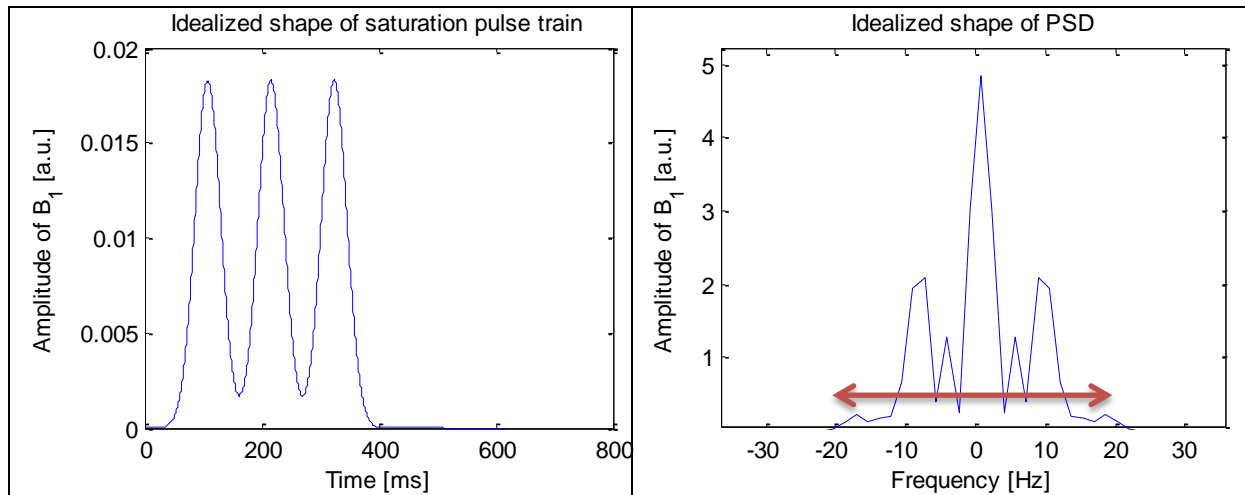


Figure 2-12 Left: Illustration of ideal saturation pulse train with Gaussian pulses as used later in the experiment. Right: The power spectral density function is just the Fourier transform of the pulse train squared. The real pulse trains are truncated giving rise to a slightly broader PSD that indicated here. Illustrations are generated in MatLab.

2.2.7 gagCEST

The chemical exchange subjects of gagCEST are the hydroxyl groups on the GAG disaccharide unit as depicted in Figure 2-3. The hydroxyl groups however are not trivial as a CEST-subject; in earlier work by Ling et al., the chemical shift of these peaks were determined through CEST and assigned to somewhere between 1 – 2 ppm [24]. However, hydroxyl NMR signals are known to vary in frequency as temperature, pH or even concentration is changed due to the electromagnetic shielding effects of hydrogen bonding [25]. Despite this, gagCEST imaging should be possible – saturation pulses do have a finite bandwidth ensuring a saturation effect is achieved even if the absorption spectra of the GAG-hydroxyls are ambiguous

2.2.8 Current state of gagCEST imaging

Most present techniques for gagCEST-imaging gather several images with saturation pulses at different shifts to produce a CEST-spectrum in each pixel which then can be analyzed over the whole or part of the range [17]. This is more flexible than comparing the effect of two different saturation pulses at positive and negative chemical shift as originally proposed by Wolff and Balaban [15].

Ling et al. came up with very promising results using the simple two image technique [3]. By immersing a piece of bovine patella in trypsin, the amount of GAG is depleted in relation to the time spent in the trypsin bath. In the article from 2007, a steady decrease in CEST signal intensity with the trypsination time is presented. Moreover, gagCEST measurements are compared to Na-23 NMR which can be said to be a gold standard in GAG measurement. In response to this, Singh et al. presented an article in which they criticized the previously positive results at 3 T. According to their claims, gagCEST effects are negligible at 3 Tesla due to direct water saturation, fast exchange rate of –OH and the masking effect of NOE; the CEST effect observed by Ling et al. was attributed to poor or nonexistent correction of B_1 inhomogeneity [17]. These two articles, however, represent a very optimistic and a very pessimistic view on current gagCEST-technique. A notable study was performed by Kim et al. in which GAG phantoms as well as human intervertebral discs were assessed with gagCEST [5]. Five GAG phantoms with concentrations between one and five percent were measured, and a linear CEST response was recorded with $r^2 = .95$. This experiment was performed with a modified turbo spin-echo sequence with a total of 49 off-set measurements, WASSR correction and a

much smaller FOV and resolution. This indicates that gagCEST is possible at 3T, contrary to the claims of Singh et al., but the two image-subtraction method used by Ling et al. may not be effective since several measurements must be performed to correct for field inhomogeneity.

3 Methods

3.1 MRI Hardware

The system used for the MRI-investigations was a Siemens Magnetom Trio 3T machine and a 15 ch tr/tx knee coil, meaning it both transmits and receives RF power. This is a key feature allowing investigation of the CEST effect, since the saturation pulses would inflict a too high SAR without local transmission. In fact, a few trials were made with a receive only head and the system could not deliver more than 3 consecutive saturation pulses without reaching SAR limits

3.2 MRI pulse sequence and CEST image calculation

The Work-in-progress package provided by Siemens is based upon a modified 3D-FLASH sequence. It is segmented to provide enough saturation for CEST contrast. Each repetition consist of a presaturation period with variable pulse train length, number of saturation pulses, pulse power, and saturation offset, as well as an imaging block, the number of k-space lines encoded in one repetition is called segments.

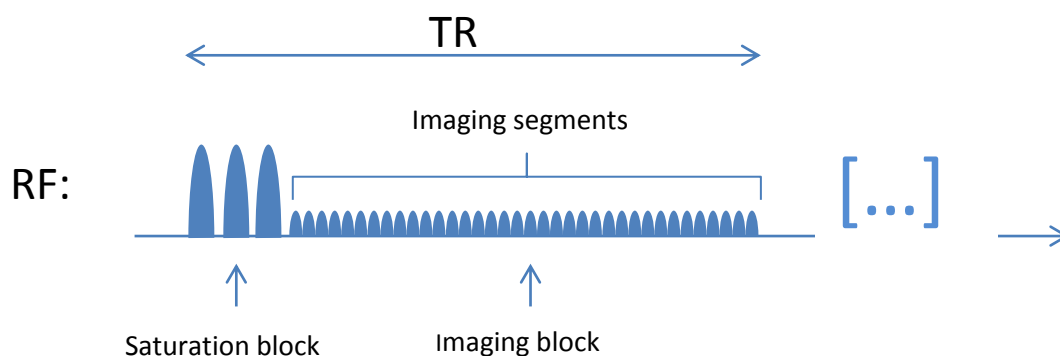


Figure 3-1 Schematic drawing of the CEST MRI excitation pulse sequence. Each “repetition” is a train of saturation pulses followed by a series of 3D-FLASH echoes. The number of echoes collected in each repetition is called segments and is typically 60-70 in a fast (ca 6 min) 3D-protocoll. The sequence is repeated until a 3D k-space is fully encoded.

To generate the CEST image a number of measurements must be performed, each corresponding to an image volume with a specific saturation frequency as illustrated in Figure 3-2. An even number of measurements must be selected where the first one is without any saturation at all, thus producing a reference image (*ref*), the following measurements (an odd number) are used to create a CEST spectrum (blue arrows in figure) where values between measurements are interpolated¹ to generate a smooth curve (red in figure). The parameter “measurements” is used to vary the number of points acquired, it is thus directly related to total acquisition time and the accuracy of the CEST calculation,. If no field inhomogeneity is present, one measurement will be done with saturation at the water

¹ Further details cannot be provided by manufacturer.

resonance, however, mostly the curve interpolation reveals a minimum shifted from the central measurement. The value of this displacement due to inhomogeneity is stored for each pixel (Inh. in figure 3-2) in a separate image volume, the inhomogeneity correction image. The CEST contrast is calculated by integrating the CEST spectrum at a positive and negative chemical shift (orange rectangles in figure) yielding the integrals $A(+)$ and $A(-)$. The parameter frequency shift is the expected chemical shift of the CEST agent, 1.3 ppm in hydroxyl gagCEST, and the delta frequency determines the width of the integrated area around this shift. The CEST value in a pixel is thus given by the following equation, where scalefactor is a simple adjustable scale factor set by the user.

$$CEST = scalefactor \cdot 2000 \frac{A(-) - A(+)}{DeltaFreq \cdot ref} + 2048$$

Ideally an image could be produced with only four measurements; one at negative shift, one at positive, one at the water frequency and one reference. However, the data processing requires enough sample points for a high quality interpolation of the complete CEST-spectrum, too few points will make this interpolation and subsequent inhomogeneity correction fail, yielding practically useless CEST images.

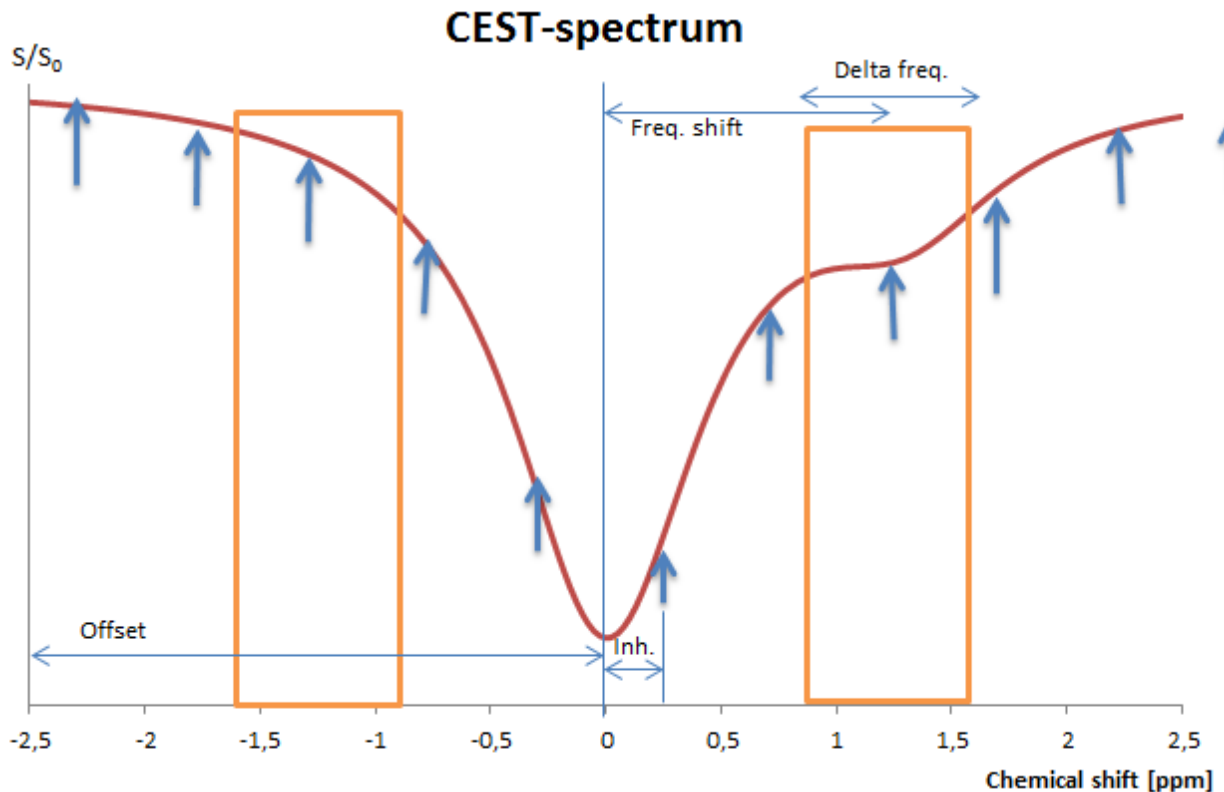


Figure 3-2 Illustration of the Siemens WIP-sequence data processing for CEST imaging. Several measurements (blue arrows) are performed starting at the offset frequency, values in between are interpolated. The curve minimum is adjusted to zero ppm and the displacement (Inh.) is stored in the inhomogeneity image for each pixel. To calculate the CEST effect the areas under the curve, inside the orange rectangles, are determined and the left and right side are compared. Depending on which CEST agent should be imaged (the chemical shift) the parameters *delta frequency* and *frequency shift* can be changed. (The presented spectrum is a simplified example)

Practically all parameters can be varied in this package, and it is not exclusively for gagCEST; e.g. the frequency shift can be set to amide groups at 2.5 ppm and the delta frequency can be set to integrate the whole spectrum.

To evaluate the CEST effect in MatLab, one slice from each measured volume is loaded as an image file. A ROI is defined in the reference image (unsaturated, anatomic image) and the mean pixel signal in this ROI is calculated for each image. These values are stored in a vector which is interpolated by inserting zeroes and performing a low pass FIR (finite impulse response) filter without altering the original values. In the current analysis the cut-off frequency of the filter is 0.5 times the Nyquist frequency of the original sampling, the filter kernel uses 2x4 original sample points for each interpolated point and the signal sampling frequency is increased by 6. This equals the input “y=interp(x,6,4,0.5)” in MatLab and gives an up-sampled CEST-spectrum for each ROI which is treated similarly to pixel based CEST calculation described in Figure 3-2. The minimal value of each vector is found and placed at zero ppm as a means of heterogeneity correction. When the CEST-spectrum is complete the CEST effect is evaluated by a generalized CEST formula similar to the one above.

$$CEST = \frac{A(-) - A(+)}{A(-)}$$

The quantity A is the area under the CEST-curve at the positive or negative frequency shift over the interval determined by the delta frequency parameter. In conclusion, the method used in MatLab is ROI based and the spectrum is created by low pass filtering and zero filling; the method used in the WIP sequence is pixel based and interpolation method is secret.

3.3 Measurements

3.3.1 Chondroitin sulfate and PBS phantoms

First measurements were performed with only GAG and buffer to test the sequence. Primary phantoms were prepared in 50 ml plastic vials containing the glycosaminoglycan polymer Chondroitin sulfate-A (Sigma Aldrich C9819), derived from bovine trachea, with phosphate buffered saline solution (Dulbeccos PBS, Sigma Aldrich), this is analogous to several other groups including Ling et al. and Kim et al. [3] [5]. Chondroitin sulfate powder was weighed using a digital scale (weight uncertainty < 1%), PBS was added to create a 5 % (wet weight, or 125 mM) solution and the mixture was stirred and heated, not boiled, until completely solved. The 5% CS solution was mixed with PBS in plastic vials to achieve concentrations of 5, 3.75, 2.5 and 1.25 percent CS simulating the actual content of cartilage as outlined in section 2.1.2. A control vial was always included in the measurement for a total of 5 vials.

Phantoms were measured suspended in a one liter bucket containing room temperature, 22°C, water left to equilibrate for at least 30 min before collection of data. The water also ensured proper coil loading and sample homogeneity and two manual 3D-shimms are performed for maximum homogeneity, according to private recommendations from Siemens technicians. Some attempts to add table salt, NaCl, to the surrounding medium was made, however, this did not affect the results in any substantial way apart from added phantom noise. The default WIP sequence settings were used, with 3 pulses 99 ms each, interpulse delay 9 ms and saturation power 2.5 μ T.

3.3.2 Low T₂ measurement with CS-A and DOTAREM

In this investigation MRI contrast agent DOTAREM, an ionic gadolinium chelate (500 mM), was used to reduce the T₂ of the surrounding fluid in the phantom, the intention was to test if the ring artifacts encountered in previous measurements would decrease due to the shortened T₂ relaxation time. Moreover, a shorter T₂-relaxation time better mirror the *in vivo* case. The same phantoms as previously were used, however, DOTAREM was added to the surrounding fluid in small increments.

The water bucket contained 450 ml of room tempered water, adding 0.45 ml DOTAREM 500 mM solution increases the concentration of the whole volume by 0.5 mM DOTAREM. The transversal relaxivity, r_2 , of DOTAREM is assumed to be 0.006 mMms⁻¹ and the relaxation time is calculated according to $T_2 = (R_2 + c \cdot r_2)^{-1}$.

Table 3-1 Volume of DOTAREM added to surrounding water and the calculated T₂. *Transversal and longitudinal relaxation times of pure water are assumed to be 2500 and 3000 ms and has minor effect on subsequently calculated values

Measurement	Amount of 500 mM DOTAREM added (ml)	T ₂ [ms]	T ₁ [ms]
1	0	2500*	3000*
2	0,45	295	429
3	0,9	157	231
4	1,35	107	158
5	2,25	65	97
6	2,70	55	81

The selected imaging parameters are the default from the WIP – that is 3 saturation pulses and 2.5 μT saturation power.

3.3.3 Chondroitin sulfate and agarose gel phantoms

Agarose-gel was added to GAG-phantoms to create more *in vivo* like conditions. An analogous set of vials was created but with agarose (Lonza, LSL LE 8200 Agarose) added together with the CS powder, and mixed with agarose/PBS to make 2 % agarose gels with varying amount of CS. The agarose would give a shorter T₂-relaxation at the expense of a broader MT-spectrum and is adopted by several other groups in the study of CEST phenomena [19, 26]. Two percent wet weight agarose would give a transversal relaxation time of 50 ms [27], closely resembling *in vivo* conditions, and ideally make the artifacts from residual magnetization go away. In addition, phantoms were immersed in 3 mM DOTAREM solution to reduce artifacts surrounding the vials. The vials were sealed with paraffin wax to prevent drying out.

To find an optimal saturation sequence three different saturation powers were chosen; the default 2.5 μT in the WIP sequence which is designed by Siemens for optimal *in vivo* imaging; 1.6 μT as specified as optimal by Zu et al. at 1000 Hz chemical exchange rate [19]; and finally 0.8 μT resembling the saturation frequency of 42 Hz utilized by Ling et al. [3]. Moreover, the default setting on the WIP sequence is a 3 pulse scheme with 99 ms saturation pulse time and intermediate spoiling, whereas Ling et al. used a 10 pulse scheme with 31 ms saturation pulse duration and intermediate spoiling [3]. The latter method could generate less residual magnetization due to the excessive spoiling, even though implying steeper gradients and higher SAR. By adjusting the number of pulses and the pulse

duration the total saturation time is kept constant which is important when comparing two methods according to Figure 2-10. This results in six different measurements presented in Table 3-2.

Table 3-2 Table of measurement parameters when investigating an optimal saturation pulse scheme.

Measurement	1	2	3	4	5	6
Number of pulses	3	3	3	10	10	10
Pulse duration [ms]	99	99	99	30	30	30
Interpulse delay [ms]	9	9	9	3	3	3
Saturation pulse CWPE [μ T]	2.5	1.6	0.8	2.5	1.6	0.8

3.3.4 Cartilage samples

Frozen femoral knee cartilage samples from the articular surfaces were provided by prof. Leif Dalhberg at the orthopedics department. The samples measured approximately 3 cm in diameter and up to 6 mm in thickness. A cartilage layer of 2-3 mm was clearly visible. They were immersed in PBS over night to rehydrate before measurements and remain at physiological pH. During imaging samples were placed in a plastic cup, which was suspended in a larger water bath to achieve proper coil loading and homogeneity. The surrounding fluid was infused with Dotarem to lower T_2 , additionally, Dotarem to a concentration of 1.5 mM was added to the plastic cup before the measurement started so that it would reduce artifacts in the fluid around the samples. Since the total scan time was less than one hour, we do not expect substantial diffusion of contrast agent into the cartilage [8].

Only the first three measurements in Table 3-2 were performed, since image quality turned out bad.

3.3.5 *In vivo* measurement with healthy volunteers

According to previous investigations a short enough T_2 is required to produce a CEST image as well as a long T_1 , both criteria should be fulfilled *in vivo*. A total of six volunteers were asked to participate in the *in vivo* evaluation of the CEST sequence. A written consent form was produced and handed to each participant together with the standard safety sheet from the MR-department. All relevant safety procedures were followed and no personal information other than sex, age, length, weight, physical activities and history of potential knee injuries were saved.

A series of measurements with the same parameters as used for imaging the agarose gel phantoms (Table 3-2) were performed on the first three volunteers. The posterior central medial femoral cartilage region (pCMF according to nomenclature suggested by Eckstein et al. [28]) was selected as ROI (see Figure 4-11) due to its high GAG content of 5 % by mass in young subjects [29]. To test the ability of the sequence to correctly measure GAG concentration, the pCMF was compared to a meniscus ROI which is clearly visible on the anatomic images. The meniscus has been shown to contain 0.3 to 0.7 % wet weight GAG [30, 31], thus, when comparing the mean CEST signal in the ROI of the pCMF and meniscus we expected a ratio in the order of ten.

One volunteer was later used to study the effect of flipping the phase encoding direction 90 and 180 degrees, as well as for evaluation of the use of fat-suppression.

The last two volunteers were imaged to gather complete datasets which were used to construct CEST-spectra in MatLab for both the meniscus and pCMF cartilage, since this data was not available from the first three volunteers.

3.4 MR imaging parameters

Imaging parameters are selected to make a time optimized and low SAR measurement. This leads to minimized resolution and large voxel size for SNR as well as relatively short sequence repetition time and saturation time. The number and amplitude of the saturation pulses are varied, whereas the total saturation time is kept constant in the experiments. The number of measurements is 14 by default and is not altered – too few measurements proved to produce bad images with too much artifacts due to poor curve fitting.

Table 3-3 Image parameters for CEST measurements, matrix resolution and number of slices were selected to minimize acquisition time.

FoV [mm]	160 x 160
Slice [mm]	3 with 12.5 % oversampling
Slices	16 (minimum number)
Matrix	192 x 192 (lowest possible)
TE [ms]	3.31
TR [ms]	618
Scan time [min]	6.04
Saturation parameters	
Offset [ppm]	2.6
Freq. Shift [ppm]	1.2
Delta freq. [ppm]	1.3
Saturation time	324-330 ms
CEST parameters	
Measurements	14
Image registration	None
Segments	64

3.5 Data processing

Most data processing was done in MatLab 7.13.0.564 (MathWorks inc.), this includes ROI-definition and manual calculation of the CEST-effect. The most basic image evaluations was done on the Siemens workstation, and in case images were already transferred to external storage media, with the freeware ezDICOM (ezDICOM medical viewer, copyright (c) 2002, Wolfgang Krug and Chris Rorden).

3.5.1 Chondroitin sulfate and PBS phantoms

The automatically generated CEST image was used first. A ROI was drawn in each vial inside a central slice and the mean CEST signal value was plotted as a function of actual GAG concentration. Next, all images were loaded and treated in MatLab according to section 3.2, whereby the calculated CEST is plotted as a function of actual GAG concentration.

3.5.2 Low T₂ measurement with CS-A and DOTAREM

No rigorous data processing was done in this step. It was only performed to test if the ring artifacts previously encountered could be mitigated.

3.5.3 Chondroitin sulfate and agarose gel phantoms

In this step, no evaluation was done directly on CEST images. The selected images (central slices) were loaded into MatLab and CEST-spectra was calculated for each series. The hope was to see a substantial difference in CEST effect between different saturation parameters.

3.5.4 Cartilage samples

Once again, images are treated in MatLab to construct CEST-spectra. The calculated CEST effect and the overall quality of the spectra is intended as a measure of the success of a saturation setting.

3.5.5 *In vivo* measurement with healthy volunteers

In the case with human subjects, motion becomes an issue. As a single CEST investigation takes approximately 6 minutes with the default time-optimized protocol used, which is a reasonable time to remain still. If motion occur within this time anyway, there is an elastic within measurement image registration. If this fails the CEST spectra is grossly disturbed and a new scan can be made. However, when comparing different saturation schemes the whole scan time is 36 minutes resulting in some movement between series. This can be corrected in MatLab by registering the different series. The function `cpselect` lets the user select anatomical control points in a reference and a distorted image; the function `cp2tform` calculates the transform needed to shift the control points in the distorted image to match the control image; finally the function `imtransform` performs the transform as illustrated in Figure 3-3. This allows one single ROI to be drawn for all series.

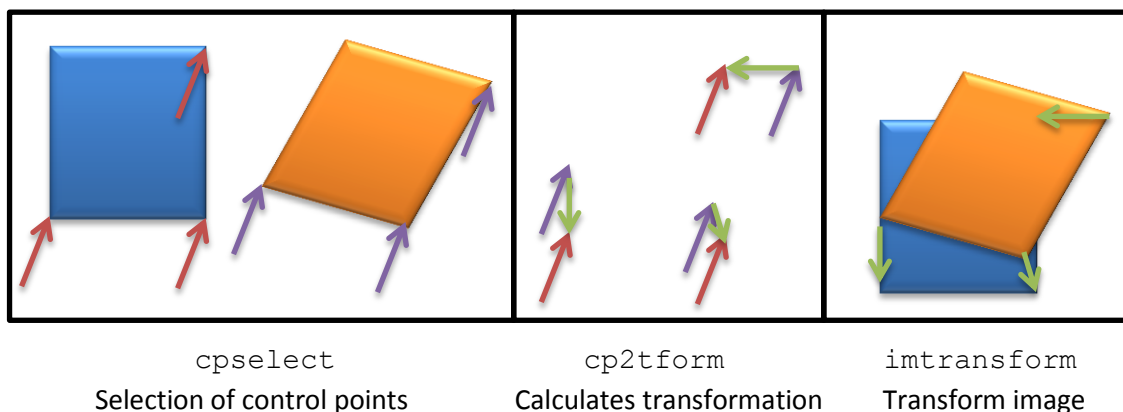


Figure 3-3 Illustration of three step image registration in MatLab

In the first three volunteers, ROIs were drawn in the CEST images produced, and the ratio $\text{CEST}(\text{pCMF})/\text{CEST}(\text{meniscus})$ is presented.

In the fourth volunteer only default CEST images are provided.

In the fifth and sixth volunteers, images are loaded in MatLab and CEST-spectra are constructed for meniscus and pCMF, in addition CEST images from all series are presented.

4 Results

4.1 Chondroitin sulfate and PBS phantoms

Pure CS-A/PBS phantoms were created according to the methods section and surrounded by room temperature water. Image parameters are presented in table 3-3. A selected slice in the middle of the phantom is presented from every 3D volume collected in the series in Figure 4-1. The series acquisition starts with an unsaturated reference volume. The subsequently acquired image volumes are obtained with selective saturation pulses at the values specified by the parameters “offset” (2.6 ppm) and “number of measurements” (14 including reference) as described in section 3.2. In the phantom GAG concentration goes from zero (bottom left), to 2.5 % CS-A (top middle) and 5 % CS-A (bottom right).

Unsaturated image	Sat. at ≈ -2.6 ppm	Sat. at ≈ -2.17 ppm	Sat. at ≈ -1.73 ppm
Sat. at ≈ -1.30 ppm	Sat. at ≈ -0.87 ppm	Sat. at ≈ -0.43 ppm	Sat. at ≈ 0.0 ppm
Sat. at ≈ 0.43 ppm	Sat. at ≈ 0.87 ppm	Sat. at ≈ 1.30 ppm	Sat. at ≈ 1.73 ppm
Sat. at ≈ 2.17 ppm	Saturation at ≈ 2.6 ppm	Correction image	CEST image

Figure 4-1 Table of all images produced from a 13 point CEST-measurement. Unsaturated reference image is top left with GAG concentration indicated, followed by the 13 images with selective saturation pulses. Inhomogeneity correction image and final CEST image, calculated according to section 3.2, are at bottom right.

A conspicuous feature of the central saturation images (sat. at 0.00 ppm), the inhomogeneity correction image and the CEST image is the elliptical pattern of profound signal variation. This led to large pixel heterogeneity even within the vials which practically made the CEST-image unsuitable for evaluating GAG content differences less than 2.5 %. Normal B_0 inhomogeneity should be accounted for by the correction method and presented in the correction image, however, the patterns remain in the CEST image is considered artefactual.

Table 4-1 Table of mean pixel value inside ROI in CEST image. baseline is 2.048

CS-A concentration [%]	0	1.25	2.5	3.75	5
CEST-effect [a.u]	2.3	2.3	3.0	3.0	3.5

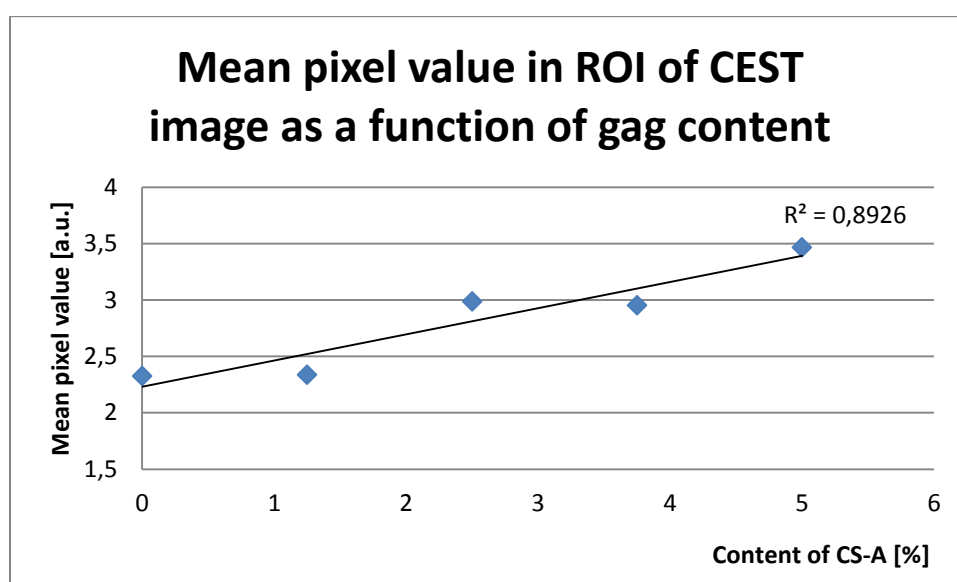


Figure 4-2 Diagram of mean pixel value in CEST image ROI as function of chondroitin sulfate concentration. Linear regression line is shown – representing an ideal case.

As can be seen in Figure 4-2 the signal intensity as a function of GAG concentration does indicate a positive trend across the whole range, though some data points indicate a decrease in signal with increasing GAG content. The uncertainty in signal intensity most likely originates in the profound signal inhomogeneity present in the CEST image caused by the circular artifacts. However, by loading all images into MatLab a new spectrum can be constructed from the mean signal in the ROI from every measurement, instead of the pixel-wise calculation. This also allows us to study the CEST spectrum of the test vials as pictured in Figure 4-3.

Since the minima are aligned in the CEST spectrum (Figure 4-3) an initial evaluation of the CEST effect can be done by looking at the spectrum to the right of the zero offset minima (positive shift in this spectrum). The successive broadening of the peaks and skewness going from zero to five percent CS-A is ideally caused by a CEST effect at 1.2 ppm. However a more rigorous calculation of the effect is

done in MatLab with the same calculation parameters as used in the WIP-software; that is a frequency shift of 1.2 ppm and delta frequency (integration length) of 1.3 ppm, results presented in Table 4-2 and Figure 4-4. The negative CEST effect in table 4.2 is a measure of the uncertainty of the investigation, the CEST effect is ideally zero if there is only water in the sample.

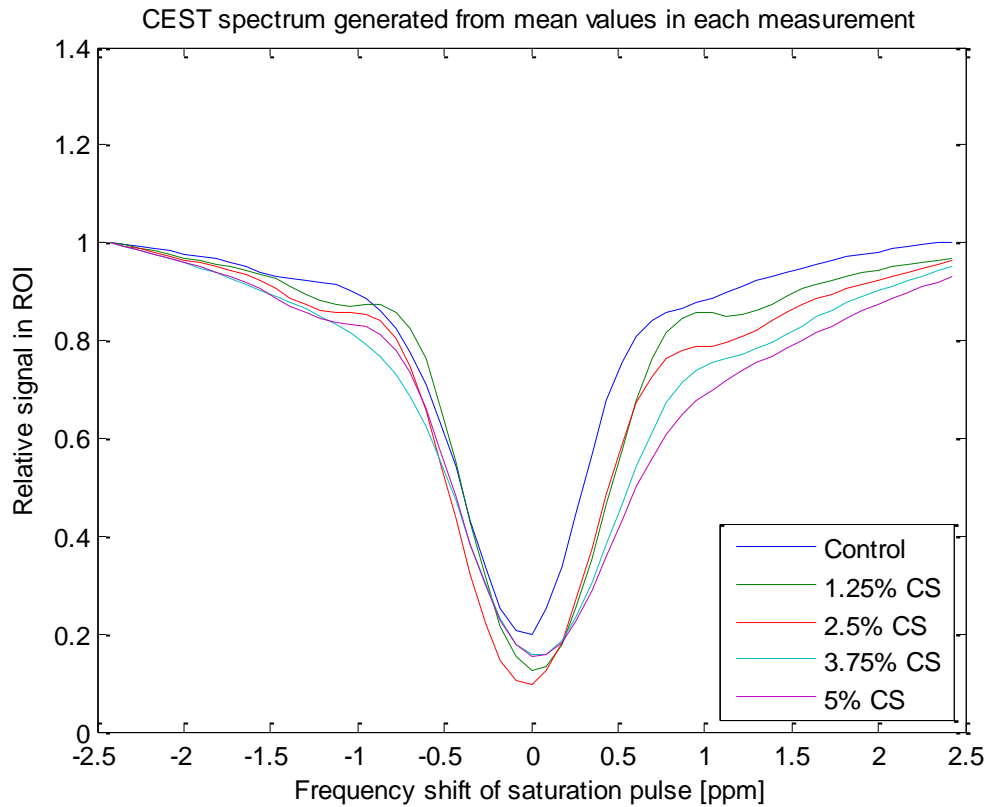


Figure 4-3 CEST spectrum generated from mean pixel intensity in ROI, curves are interpolated from 14 measurements, normalized and aligned with minima in center.

Table 4-2 Table of calculated CEST effect and GAG concentration

CS-A concentration [%]	0	1.25	2.5	3.75	5
Calculated CEST	-0.021	0.042	0.049	0.086	0.15

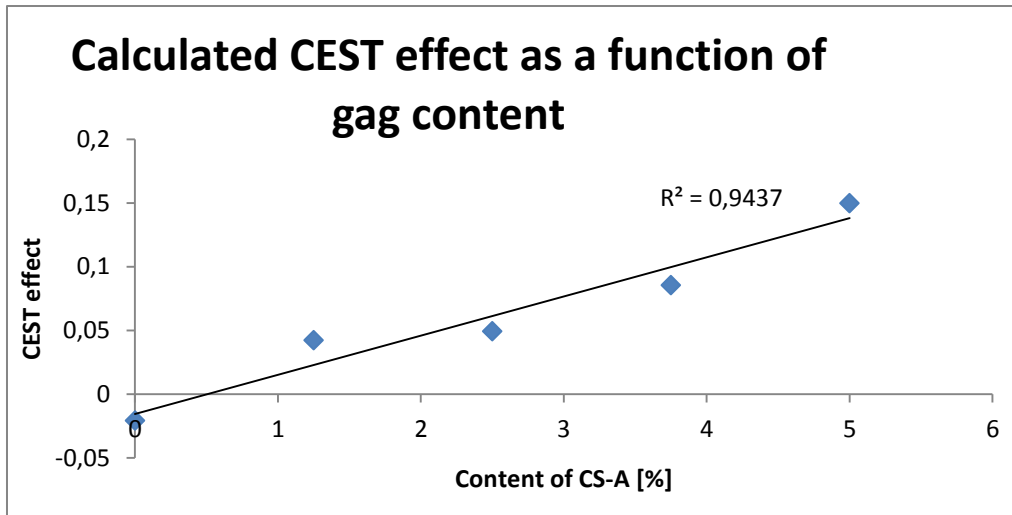


Figure 4-4 Diagram of calculated CEST effect (see methods section) as a function of GAG-content in five vials. A linear regression is included

4.2 Low T₂ measurement with CS-A and DOTAREM

An attempt was made to reduce the circular artifacts by adding MRI contrast media to the surrounding fluid. Acquisition of gagCEST images with default parameters, 3 pulses, 2.5 μT and DOTAREM added to the surrounding water.

<p>MR037-001-009.dcm C: 2048 W: 4089</p>	<p>MR056-001-009.dcm C: 2047 W: 4095</p>	<p>MR075-001-009.dcm C: 2047 W: 4095</p>
Control measurement	0.5 mM DOTAREM	1.0 mM DOTAREM
<p>MR094-001-009.dcm C: 2048 W: 4089</p>	<p>MR114-001-009.dcm C: 2047 W: 4095</p>	<p>MR133-001-009.dcm C: 2047 W: 4095</p>
1.5 mM DOTAREM	2.5 mM DOTAREM	3.0 mM DOTAREM

Figure 4-5 Table of CEST images from “low T₂ measurements.” The vials contain PBS and CS-A, the surrounding fluid is water with varying concentration of DOTAREM which lowers the relaxation times.

It is clear from a visual evaluation of the images that the artifacts are reduced and the pattern is more random in the measurements with 1.5 mM or higher concentration DOTAREM. This corresponds to a transversal relaxation time of less than 100 ms which is more resembling of an *in vivo* situation, such as cartilage. On the other hand, the signals inside the vials containing CS-A is still very variable.

As a final resort DOTAREM was added to the test tubes containing variable amounts of CS-A, this would ideally create a phantom without artifacts suited for reference gagCEST measurements. Conversely, the contrast agent also lowers the longitudinal relaxation rate as can be seen in Table 3-1, this means the saturation effect of the CEST pulse is completely removed and no CEST contrast is visible in the images. An alternative route at this point was to lower the number of segments per shot (FLASH read outs after each saturation) which allows more signal to be retained during the imaging block. Images with 72 and 25 segments gathered between saturation pulses are presented in Figure 4-6

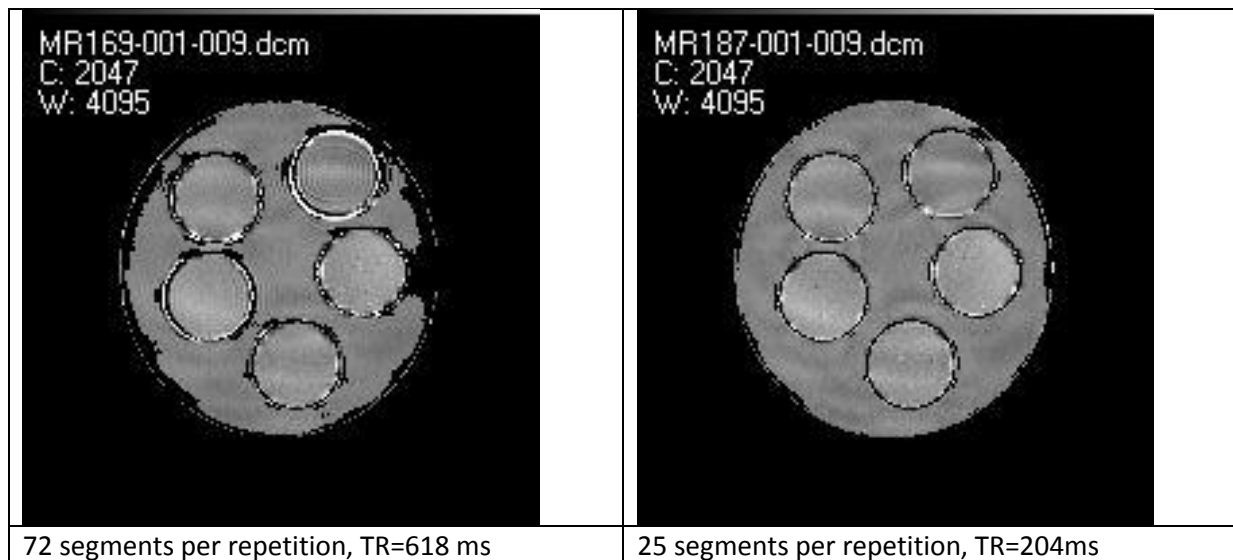


Figure 4-6 Measurement of CS-A in PBS with 1.5 mM DOTAREM (vials) immersed in 3.0 mM DOTAREM solution

4.3 Chondroitin sulfate and agarose gel phantoms

In order to decrease T_2 and reduce artifacts, vials were prepared according to the methods section containing a fixed amount of agarose as well as variable amounts of CS-A. The CS-A concentration of the vials in the phantom are indicated in Figure 4-7. The surrounding fluid is water with 1.5 mM DOTAREM.

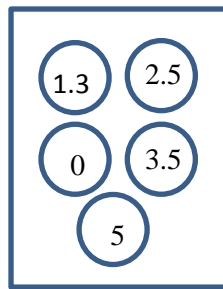


Figure 4-7 Placement of agarose and CS-A vials (as a reference for Figure 4-8), numbers indicate concentration of CS-A in wet weight.

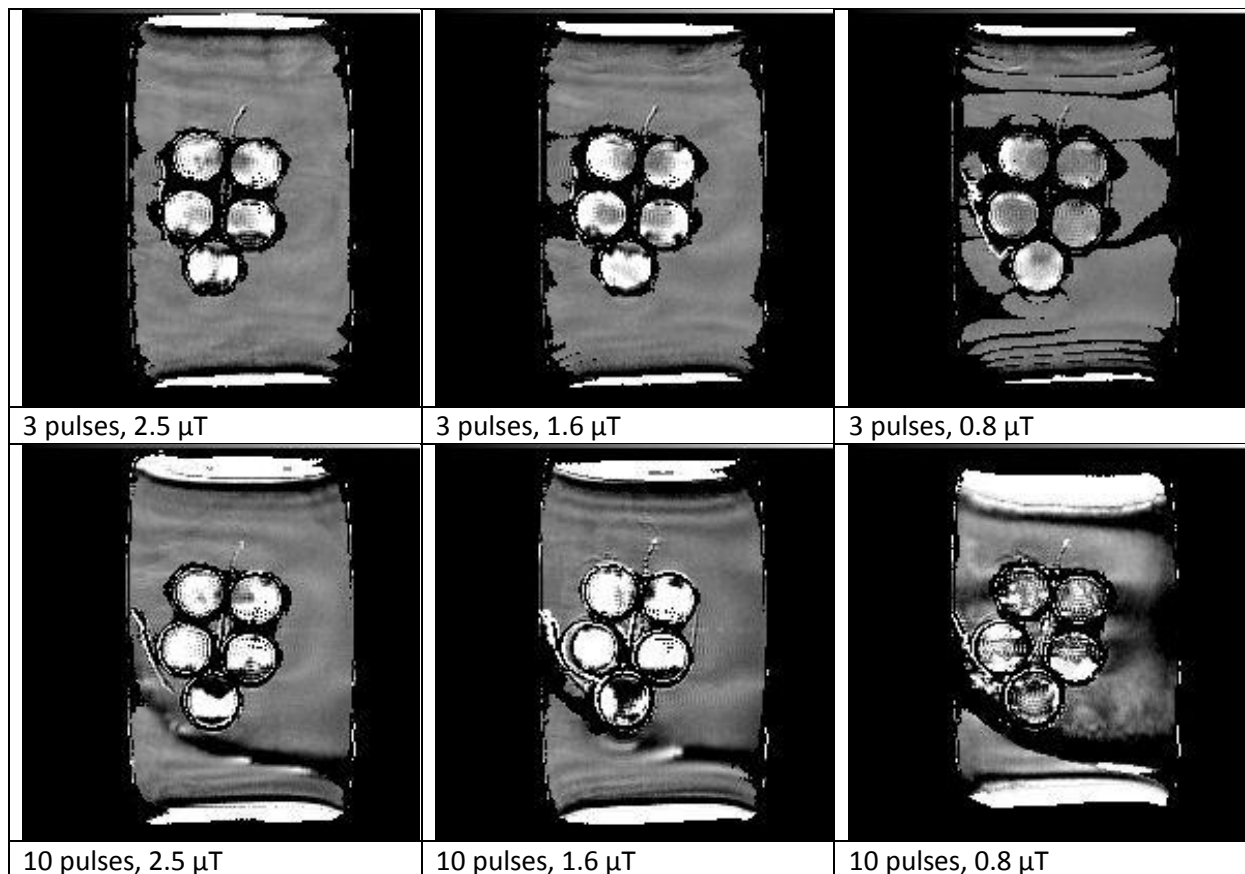


Figure 4-8 Table of CEST images from agarose + CS-A measurements, GAG concentration . Six different saturation techniques were employed.

As can be seen in Figure 4-8 large heterogeneity still remains inside and around the vials in the CEST images. As in the earlier experiment a trial was made to construct a CEST spectrum using the raw data from all gathered images and defining a ROI in each vial. The spectra created are presented in Figure 4-9. Only the measurements with 3 pulses, 0.8 μ T and 3 pulses, 1.6 μ T could be interpolated and corrected. The other four measurements are presented raw as 13 points with varying mean signal intensity in the pixels. This is the case since the correction function requires a global minima, close to the center of the spectrum – otherwise the required inhomogeneity shift is larger than the “frequency shift” parameter as shown in Figure 3-2.

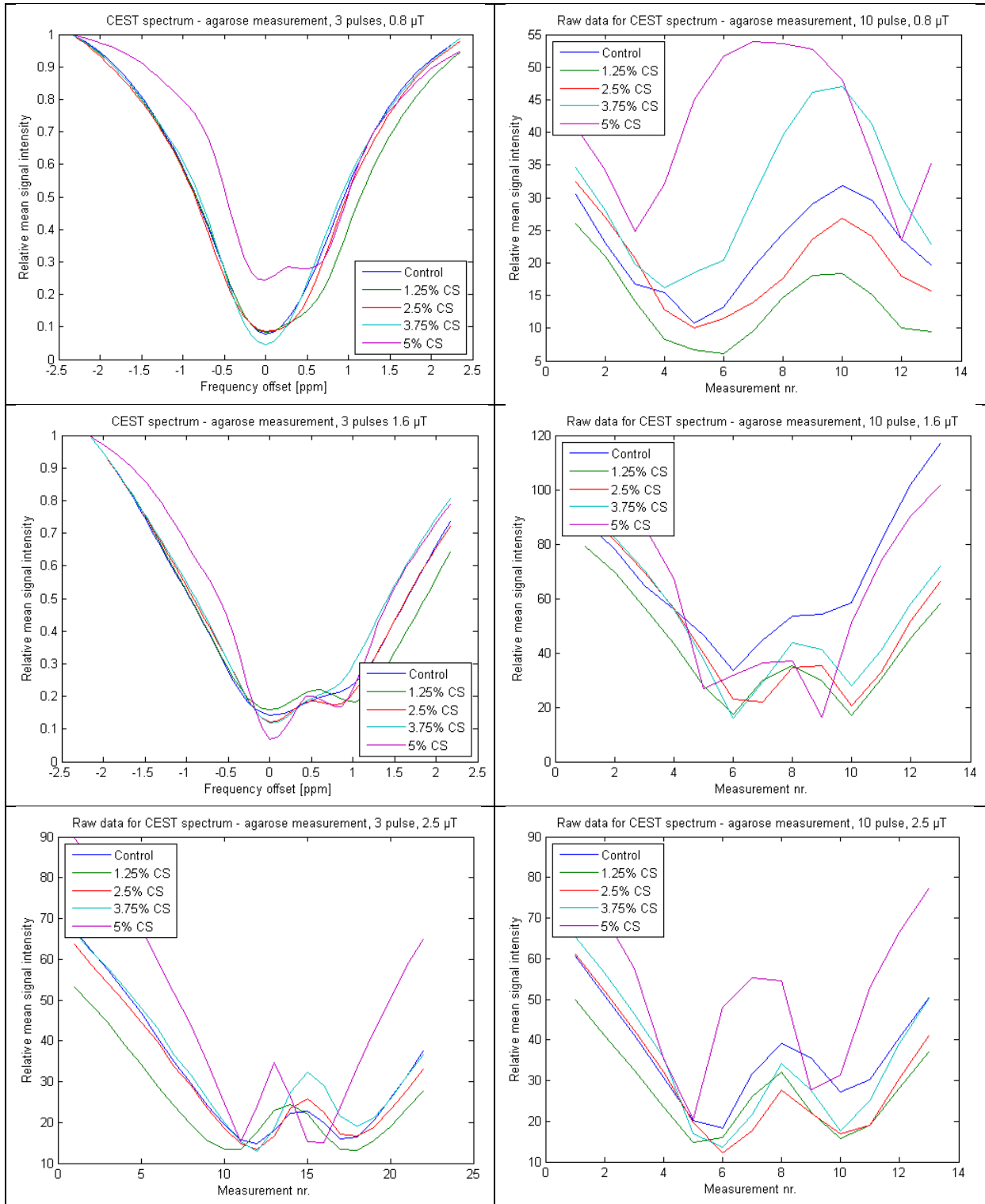


Figure 4-9 Calculated CEST spectra (top and middle, left) and raw data (the rest) from measurements on vials containing 2% agarose and various amount of CS-A for 6 different saturation schemes. Left column shows the 3 pulse series and right column is the 10 pulse series. Top row is 0.8 μT CWPE, middle 1.6 μT and bottom row 2.5 μT . some measurements could not be interpolated and corrected due to double minima.

4.4 Cartilage sample measurements

Freeze dried cartilage samples for CEST measurements were provided by the orthopedics department in order to optimize the saturation parameters. CEST contrast was observed in all samples and images, and the CEST effect was evaluated by constructing spectra in MatLab, based on ROI:s drawn in the unsaturated images where cartilage is well visible as in figure 4-10. The CEST values are presented in Table 4-3. The three CEST images produced automatically as well as the corresponding calculated spectra are displayed in table 4-4. No difference between samples are expected.

Table 4-3 Calculated CEST effect in two samples of articular cartilage as a function of three different saturation CWPE.

Saturation CWPE:	0.8 μ T	1.6 μ T	2.5 μ T
Bottom sample CEST	0.0021	-0.091	0.015
Top sample CEST	-0.031	-0.061	-0.0032

No conclusions can be drawn from this investigation regarding the optimization of saturation pulse power. One should expect to obtain heterogeneous CEST contrast within cartilage sample since the concentration of GAG varies over the cartilage surface. This seems to be true for all measurements; however, the signal variation within cartilage is of the same magnitude as the signal variation in the surrounding water. Though the cartilage samples are at all times discernible with a previous knowledge of their position, they almost blend into the surrounding. Whether the CEST contrast originates in the true dispersion of GAG concentration or if it originates in field inhomogeneity must yet be determined. This makes relative measurements of CEST signal within the images difficult. The success of a saturation pulse is rather measured as the calculated CEST effect from the spectra produced in MatLab. However, this is also complicated by the presence of heterogeneity.

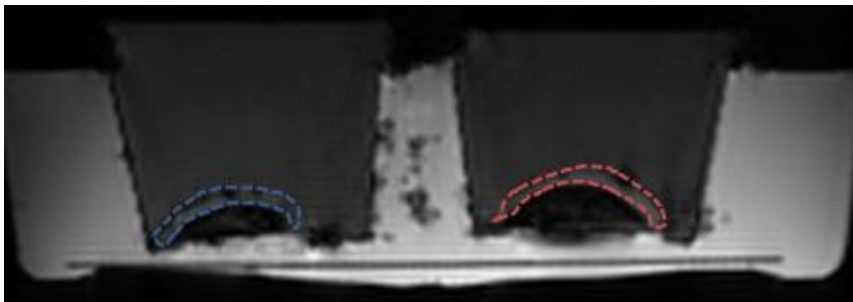
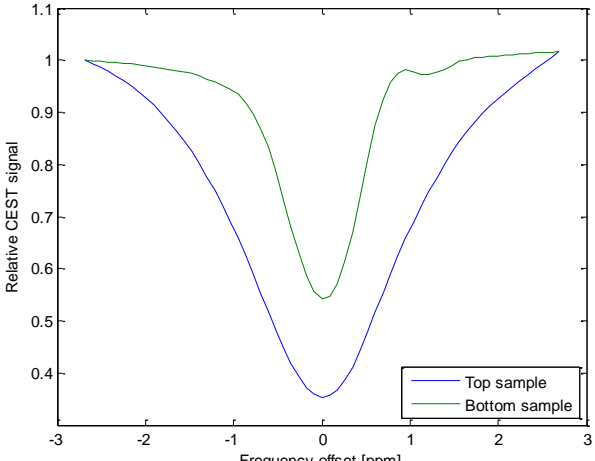
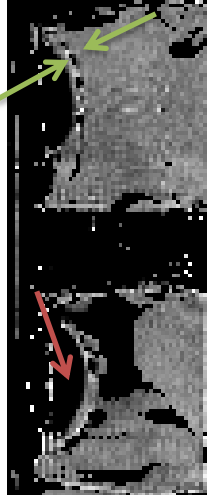
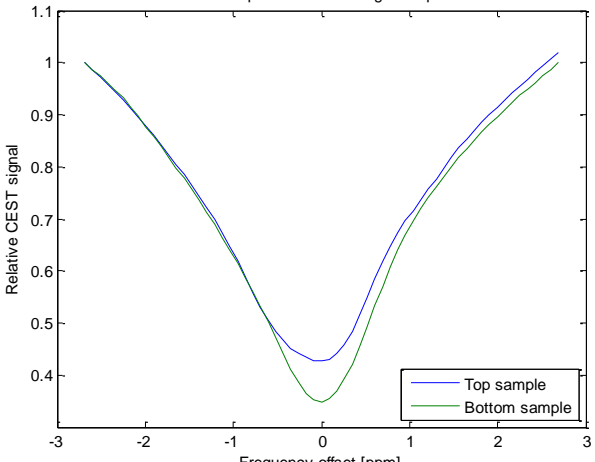

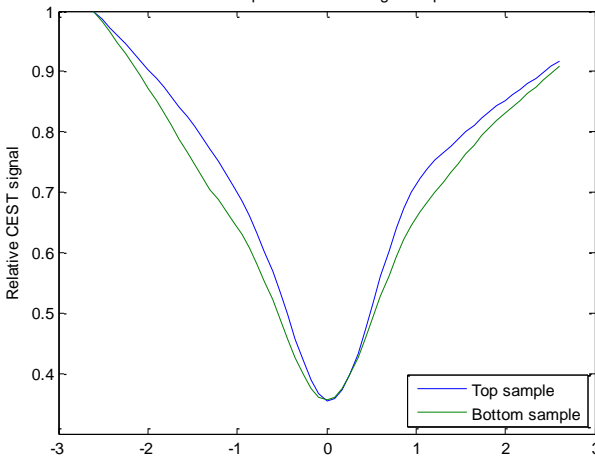



Figure 4-10 ROIs used for measurement of cartilage gagCEST-effect in table 4-4. Blue ROI is “top” sample and red ROI is “bottom” sample.

Table 4-4 Calculated CEST spectra and CEST images of cartilage samples at three different saturation CWPE values. In 0.8 μ T image, green arrows show cartilage region and red arrow point at the condyle bone.

	CEST spectra calculated in MatLab	CEST image
0.8 μ T	 <p>CEST-spectra from cartilage sample</p> <p>Relative CEST signal</p> <p>Frequency offset [ppm]</p> <p>Top sample Bottom sample</p>	
1.6 μ T	 <p>CEST-spectra from cartilage sample</p> <p>Relative CEST signal</p> <p>Frequency offset [ppm]</p> <p>Top sample Bottom sample</p>	
2.5 μ T	 <p>CEST-spectra from cartilage sample</p> <p>Relative CEST signal</p> <p>Frequency offset [ppm]</p> <p>Top sample Bottom sample</p>	

4.5 *In vivo* measurement with healthy volunteers

In vivo measurements were performed with healthy subjects in order to test the sequence. CEST images are displayed as a red colormap on top of the anatomical measurement from the first series. In the images, tissue with GAG or other agents exhibiting chemical exchange (such as proteins in general) are painted red with intensity matching the concentration – muscles, skin and cartilage specifically. The measurement is presented in Table 4-5.

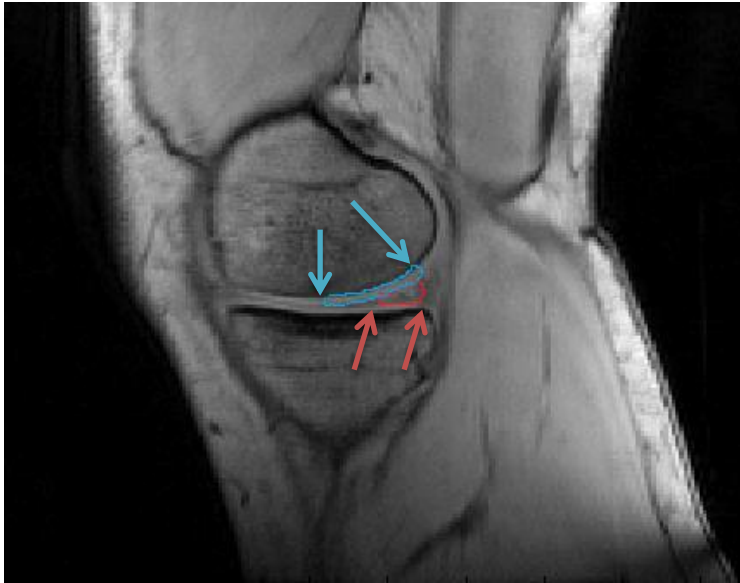


Figure 4-11 Defining ROI for pCMF (blue) and meniscus (red), in subject 2.

Table 4-5 Ratios of mean CEST signal in ROI for pCMF cartilage and meniscus in 3 subjects for 6 different saturation schemes – GAG content ratio is approximately 10 in healthy subjects.

Series	1	2	3	4	5	6
Subject 1	0.92	0.75	0.81	0.99	0.55	0.64
Subject 2	0.98	1.0	1.1	1.1	1.1	1.0
Subject 3	1.2	1.0	0.80	0.70	0.95	0.83

The registered CEST-images were more closely examined with respect to motion artifacts and misregistration due to the unexpected ratios from the pCMF/meniscus measurements. However, subjects 2 and 3 proved to remain still during the whole scan time when comparing the unregistered and registered images and the registration allowed an acceptable fit even for subject 1. The registration results and unregistered images for the last series are shown for all subjects in Figure 4-12. It is still evident from visual inspection that there is in fact no CEST signal at all in the femoral articular cartilage - there is no red overlay in the pCMF region which is outlined in figure 4-11.

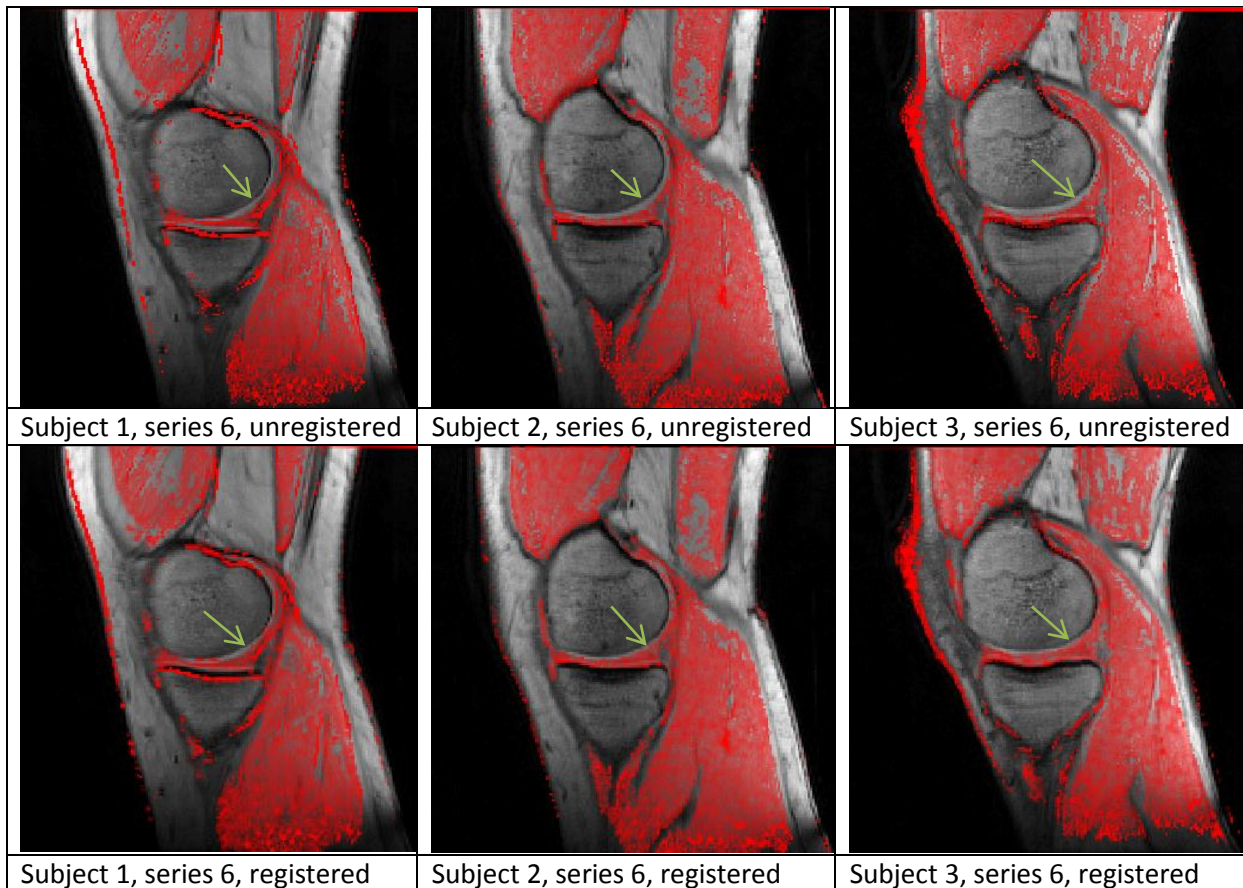


Figure 4-12 Unregistered and registered CEST-images from the last series of measurements displayed on anatomic scan for all subjects. Subjects 2 and 3 have remained still during the scan, subject 1 has moved but images are registered to a good fit. Green arrows point at pCMF region.

The CEST signal which is “missing” has disappeared in the frequency encoding direction, i.e. in the same direction the fat signal is chemically shifted. A regular 3 pulse 2.5 μT CEST measurement was performed on a volunteer and compared with the same sequence with fat-sat. The images are displayed in Figure 4-13. The ratio of pCMF/meniscus ROI mean signal is increased from 0.8 in the regular measurement to 1.1 with fat saturation, which is a positive but unsatisfactory result. Most likely the fat signal is disturbing the CEST measurement. This is conveniently circumvented by shifting the phase encoding direction from AP to PA which is equivalent to a frequency encoding direction shift of 180° on the machine.

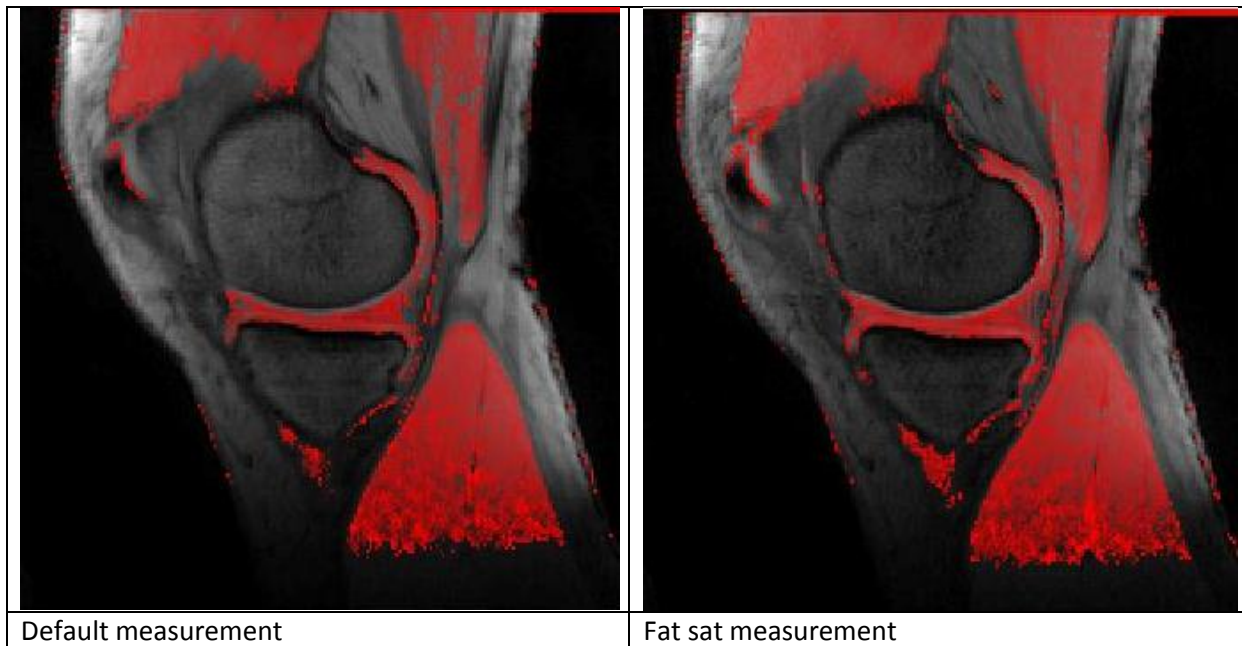


Figure 4-13 CEST images from subject 4, the regular 3 pulse, 2.5 μ T saturation is used in both. Right image has an additional selective fat saturation pulse.

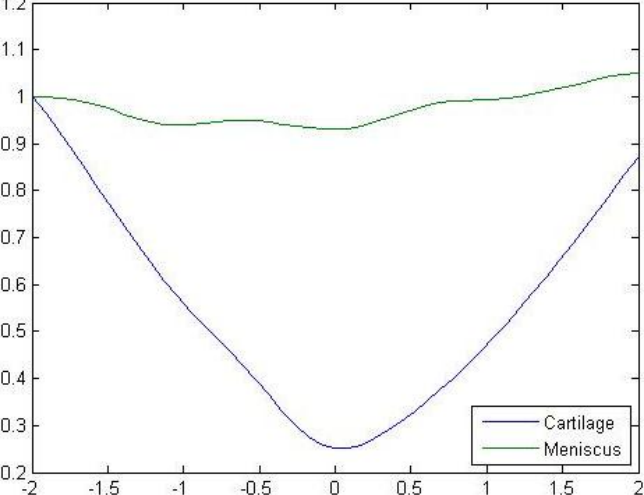

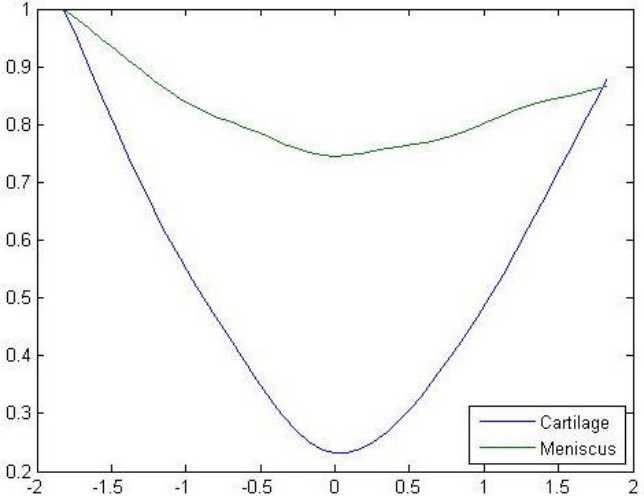

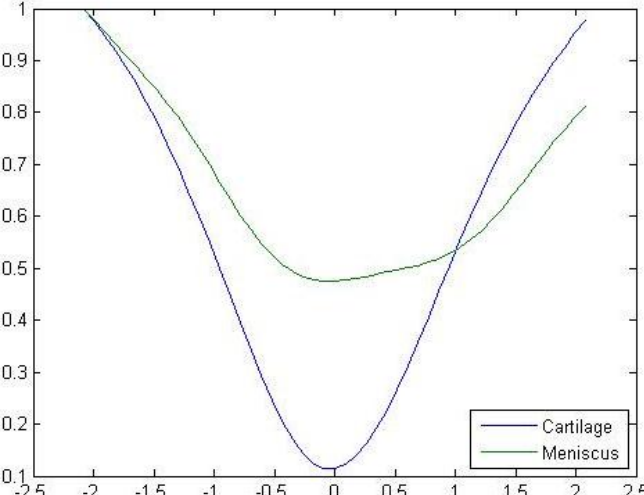

A full series of measurements according to Table 3-2 was therefore acquired for two more subjects. The mean signal ratio between pCMF and meniscus are measured from the CEST images and presented in Table 4-6, additionally all calculated CEST spectra and the produced CEST images are displayed in Table 4-7

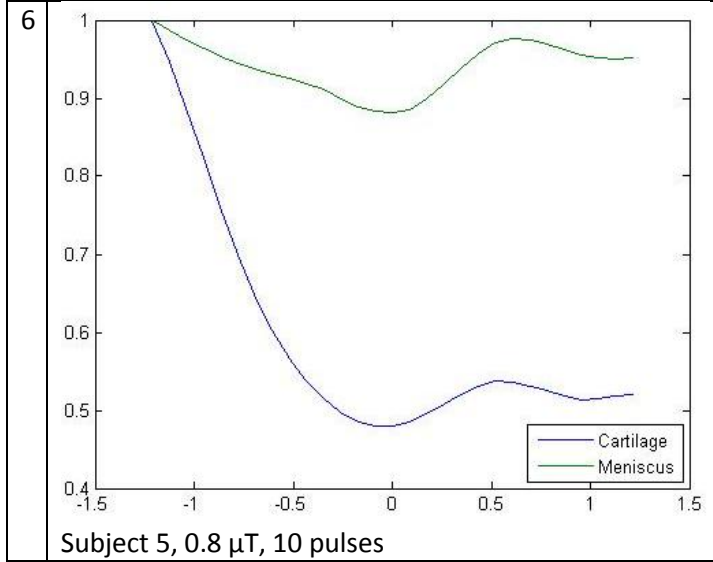
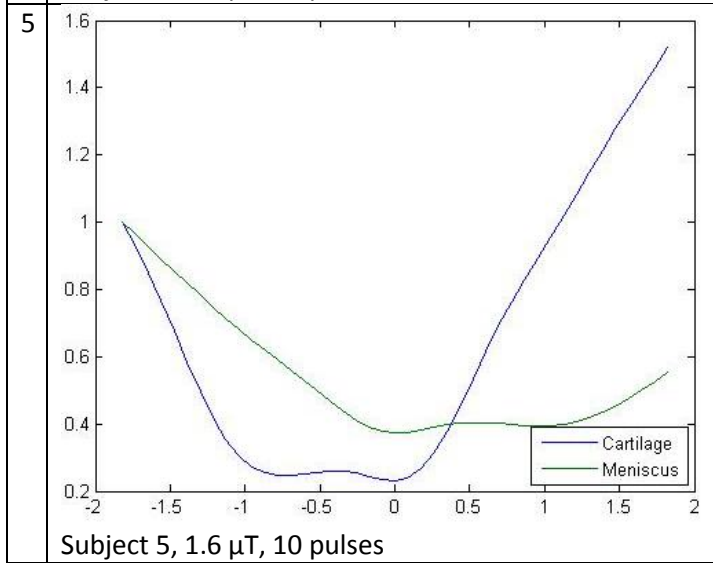
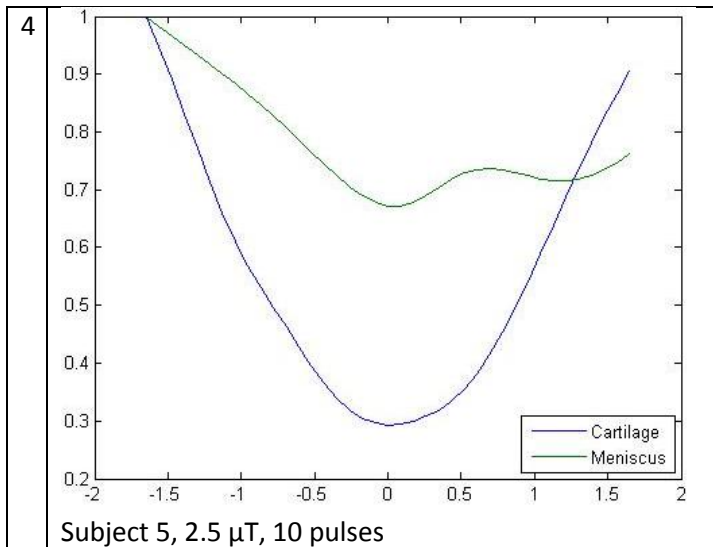
Table 4-6 Ratios of mean signal in ROI for pCMF cartilage and meniscus in 2 subjects

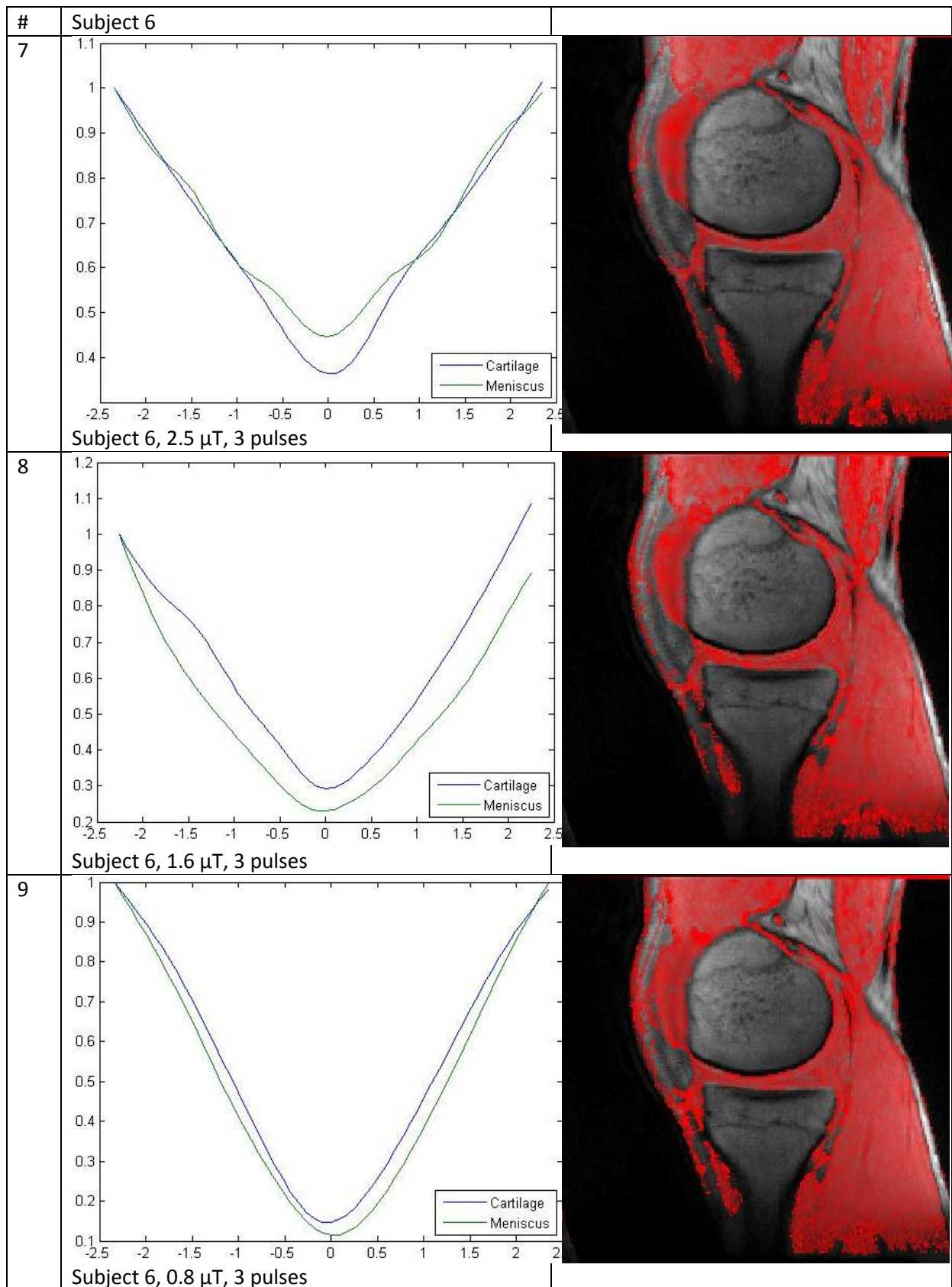
Measurement	1	2	3	4	5	6
subject 5	0.9935	0.7926	1.2195	0.9599	0.9884	1.0754
Subject 6	1.0079	0.9988	1.3618	1.0487	1.1595	1.0854

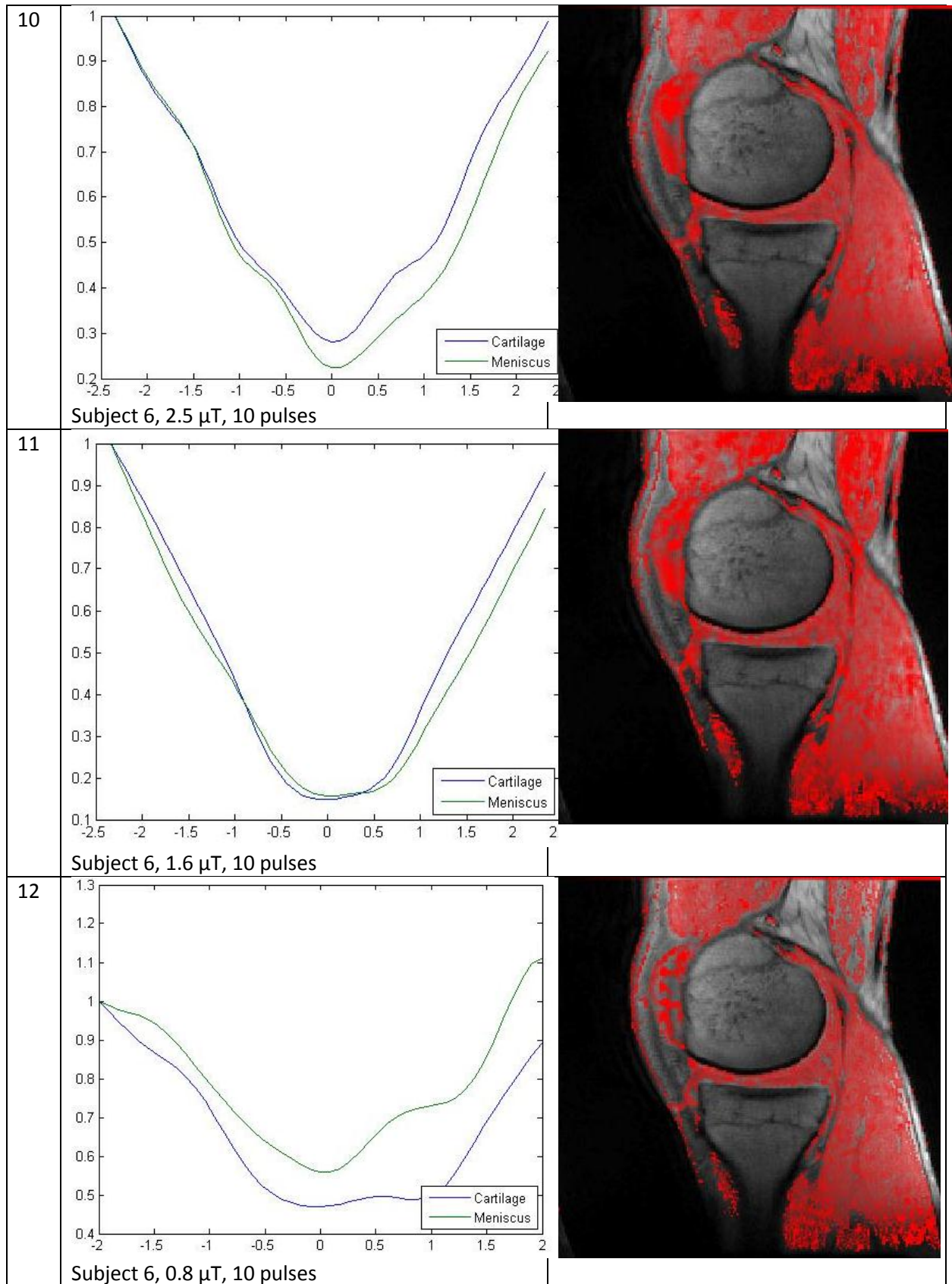
The presented experiments imply that measurements are not completely reliable. The pictures of subject 6 has a clearly visible meniscus and no chemical shift artifacts, still the spectra in Table 4-7, # 7-12 are not at all resembling the CEST spectra presented in Figure 4-3. One observation is the gross asymmetry and dual minima of the 10 pulse CEST spectra, most prominent in Table 4-7 # 6 and 12. In fact all measurements with 10 pulses seem rather unstable considering phantom measurements presented in Figure 4-9. A special case is # 5 in the same table, it seems a misregistration has occurred where the cartilage spectra has been displaced 1 ppm. Due to the correction algorithm the minima should be aligned at 0 ppm, however, the spectra is distorted due to residual magnetization or inhomogeneity causing it to display a signal loss at - 1 ppm. One observation, however, is that the CEST signal in the images produced in the 10 pulse series are more inhomogeneous than the 3 pulse equivalents, all which are presented in Table 4-7.

Table 4-7 Table of calculated CEST spectra as well as CEST images for subjects 5 for six different saturation schemes.

#	Calculated CEST spectrum – blue for Cartilage and green for meniscus, vertical axis relative mean signal, horizontal axis frequency shift in ppm	CEST images in red mask superimposed on anatomical measurement from each series, central image of 16 slices.
1	 <p data-bbox="231 907 542 929">Subject 5, 2.5 μT, 3 pulses</p>	
2	 <p data-bbox="231 1444 542 1467">Subject 5, 1.6 μT, 3 pulses</p>	
3	 <p data-bbox="231 1982 542 2004">Subject 5, 0.8 μT, 3 pulses</p>	







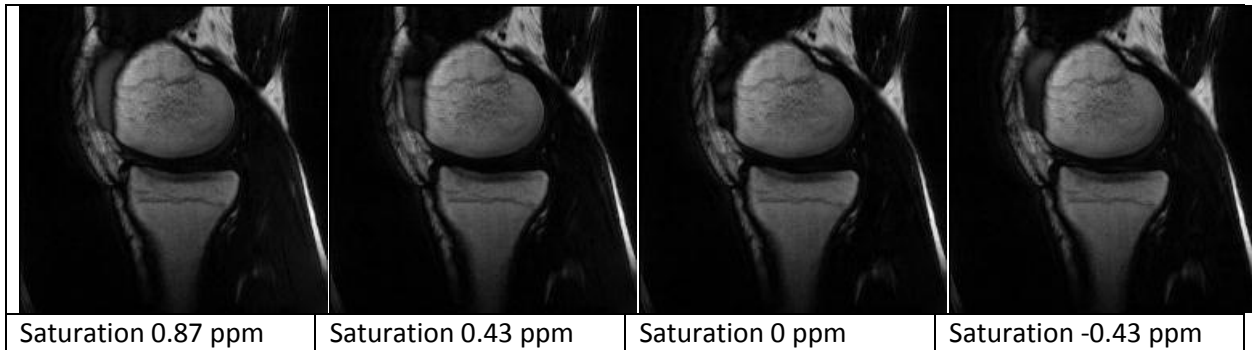


Figure 4-14 Raw images no. 6-9 from subject 6, 3 pulses, 2.5 μ T images. Residual magnetization effects are visible in the slightly enlarged bursa of the femoral condyle

By scrutinizing the raw data images from the last three volunteers it was possible to find some residual magnetization effects in the *in vivo* case as displayed in Figure 4-14. In one subject the bursa was slightly enlarged and an inhomogeneous signal was recorded in the homogeneous liquid filled region, similar effects could not be seen in subjects without enlarged bursa. The subject in question and a clinical radiologist were informed of the condition.

5 Discussion

The aim of this master dissertation was to gain understanding of the gagCEST technique through practical trials and literature study, as well as to evaluate the gagCEST method as provided in Siemens' WIP package. The practical side has incorporated phantom measurements, *in vitro* cartilage sample measurements and volunteer subjects. All measurements have proven to be severely hampered by complex residual magnetic effects and sample heterogeneity. Due to the small chemical shift of the GAG hydroxyls these effects make measurements excessively difficult. However, in all stages of the investigation, CEST signal has been recorded and attributed to the presence of GAG, indicating a potential for the technique.

5.1 Discussion of results

5.1.1 Chondroitin sulfate and PBS phantoms

The very first study proved to be one of the more successful ones. By comparing the mean CEST signal recorded in the vials, a nearly acceptable correlation with GAG content could be observed. By using MatLab to create CEST-spectra an even more compelling CEST effect could be seen, with linear correlation between CEST effect and GAG content and $R^2 = 0.94$.

Kim et al. constructed nearly identical phantoms with PBS buffer and CS in 5, 4, 3, 2 and 1 % concentration and recorded a linear correlation with gagCEST signal and $R^2 = 0.95$ [5]. However, they used a single slice TSE based technique, with slightly longer total saturation time (500 ms) and longer repetition time (2 s) to allow better restoration of magnetization between excitations. These two parameters may give better SNR in CEST measurements, moreover, they used parallel imaging to accelerate acquisitions with a factor of 2, an option not considered in this thesis.

In communication with physicists at Siemens currently developing the imaging sequence, the encountered artifacts have been confirmed to be known and are said to originate in residual magnetization which is not entirely spoiled after the saturation pulses. This could be corrected by lowering the T_2 relaxation time of the phantoms, forcing residual magnetization to dephase before

the imaging sequence. Present phantom GAG-measurements will otherwise be hindered by noisy and inhomogeneous images. A set of measurements, performed to test and confirm this hypothesis is included in Appendix 7.1.

5.1.2 Low T_2 measurement with CS-A and DOTAREM

The key to make a gagCEST phantom for the WIP sequence must be to lower the T_2 inside the test tube, with retained long T_1 . Phantoms could then be used for calibration of the gagCEST signal. Gadolinium based contrast did remove the most gross artifacts and rendered the CEST images smoother, however, it also lowered the longitudinal relaxation to the point where T_1 was as low as 150 ms in the vials, whereas the *in vivo* longitudinal relaxation has been shown to be in the order of 700 ms in the medial femoral cartilage, with values between 400 and 1000 ms not uncommon in joint cartilage [32]. This consideration makes it unnecessary to pursue further efforts in devising a CEST protocol for low T_1 phantoms, and thus another agent than Gd-based contrast should be tested.

5.1.3 Chondroitin sulfate and agarose gel phantoms

The raw data presented in Figure 4-9 exhibits profound asymmetry but is excessively difficult to interpret. Whether the saturation spectra reflect a true CEST effect, phantom inhomogeneity or ill adjusted 3D shim is not possible to tell. The fact that a small 3D-shim box, covering only the vials and not the whole volume, was used, may have caused the water frequency to be ambiguously defined, disturbing the measurement. Although the agarose concentration (2 % wet weight) will affect the magnetization transfer in the sample and induce a broader spectrum than Figure 4-3, the effect is assumed to be close to completely symmetric [26] (the MT broadening can be seen by comparing Figure 4-3 and the top left spectra in Figure 4-9).

Several authors have successfully used agarose in CEST experiments to simulate physiological parameters, however, few are interested in GAG molecules and other CEST agents with similarly small chemical shift (e.g. creatine amide at 1.9 ppm [23]). The MT effects of agarose has been investigated and confirmed to result in a broad MT spectrum where the asymmetry caused by CEST is made hard to discern. Though it should be possible to see a CEST effect despite broad MT effects in a GAG/agarose phantom, the preparation required to make these phantoms was more tedious than expected. The mixture of CS-A and agarose became very sticky and required extensive stirring and heating to dissolve, and visual inspection revealed that several samples were inhomogeneous. Due to macromolecular MT effects and the risk of creating heterogeneously mixed phantoms, agarose gels might be unadvisable as gagCEST phantoms. As a future possibility, SPIO particles (superparamagnetic iron oxide) could be tested. These should predominantly lower transversal relaxation and thus has potential for creating a CEST phantom.

5.1.4 Cartilage samples

The idea with performing measurements with cartilage samples was to test the WIP sequence in a situation even more resembling that of *in vivo*. However, one retains all heterogeneity issues from the phantom measurements, as well as adding uncertainty regarding the actual GAG content of the cartilage. Since the condition of the samples was unknown no comparison can be made between the samples in a single measurement. Additionally, comparison between two measurements performed at different times is hindered due to adjustment of shimming coils. This inability to evaluate what is a positive response in a CEST experiment obstructs the whole optimization process. It is tempting to believe a substantial CEST effect is observed in the green curve (bottom sample) at 0.8 μ T, however, this is most likely a reconstruction artifact from the interpolation. The spectra quality was not good

overall, and the calculated CEST-effect was negligible ($< 0.1\%$), possibly due to spillover effects from the surrounding medium, or the penetration of contrast agent into the cartilage, a process which is assumed to take a few hours, but could have substantial effect on CEST contrast .

5.1.5 *In vivo* measurement with healthy volunteers

Finally, the reason for doing experiments on healthy participants was to investigate if the artifacts encountered *in vitro* would persist under physiological conditions, regarding residual magnetization and heterogeneity. In fact, the relaxation properties of cartilage do make it a good candidate for CEST measurements and CEST signal could be observed in cartilage, without any prominent residual magnetization artifacts. Among all volunteers, a small residual magnetization effect can only be observed in the raw data set of subject 6, anteriorly of the femoral condyle. The homogeneous liquid filled bursa appears inhomogeneous in the CEST images. It is likely that the transversal relaxation time of the liquid filled bursa is longer than in the cartilage, making these effects of minor importance in present case, but further investigations should include a complementary T2-mapping to account for these effects.

However, the ratio of signal in the central medial femoral cartilage region and meniscus did not reflect the actual ratio of GAG content. This may be partly attributed to the heterogeneous composition of the joint – cartilage is adhered to bone, containing fat, whereas the meniscus is surrounded by cartilage, containing water. Though this can be circumvented by knowing the chemical shift, one is limited to a smaller region for measurements in the cartilage and a larger uncertainty which is a drawback when comparing different regions of the cartilage. Still, this may be the preferred method to optimize the CEST sequence *in vivo* since the constructed CEST spectra are too distorted to use as an optimization goal-function. Published articles have dealt with a comparison between gagCEST and sodium imaging *in vivo* without finding any significant correlation ($r^2=0.4$, [4]), so there is no consensus regarding the interpretation of gagCEST images of human knee cartilage. To optimize the sequence *in vivo*, one must determine a way to rate the quality of images with respect to CEST effect.

One important issue is the MT behavior of the meniscus. Its content of collagen fibers is slightly different than the cartilage, with type I collagen being dominant in menisci and type II dominating in cartilage. Moreover, the CEST spectra of the menisci seem more flat in general – specifically spectra 1 – 6 for subject 5 in Table 4-7. It is important to remember all spectra are normalized, but there are two possibilities if the effect is real, and not artifactual; either the saturation effect in the meniscus is smaller, due to denser macromolecule constitution and thus shorter T_1 relaxation; or the MT spectra is simply broader, due to higher macromolecule content and thus shorter T_2 . It is all very difficult to interpret.

5.2 Clinical future

The sequence as implemented and used in this project is not ready for clinical application. The current version is provided as a “work-in-progress” research utility from our MR scanner manufacturer, Siemens. However, as soon as a reasonable low detection limit *in vivo* has been established, the sequence will be useful for routine investigation or potential screening of GAG signal; given that there is also a method for referencing or absolute quantification. Compared to the previously employed gadolinium based cartilage imaging [2], a 6 minute scan is an attractive alternative. Even if gagCEST proves to be too complicated to use due to field heterogeneity in the knee joint, or lack of absolute quantification, CEST imaging has further potential. Chemical exchange rate is greatly influenced by pH, making it an attractive parameter to measure using CEST. *In vivo* applications of pH-CEST use the surrounding tissue as reference, making absolute quantification unnecessary, and application in investigation of brain hypoxia is already under way [33]. Moreover, the introduction of clinical 7 T scanners are believed to greatly improve gagCEST and CEST measurements due to increased chemical shift and longer T_1 [17].

5.3 Improvements and further studies

As previously stated it would still be interesting to create a reference gagCEST phantom with known relaxation times and pH. Such a phantom would allow optimization of saturation time, pulse type and power, a properly prepared agarose phantom may suffice, but alternative routes to lower T_2 should be investigated.

Another important topic is the choice of method for finding the center frequency in the CEST spectrum. The current examination is entirely based on the WIP sequence (as supplied by our MR scanner manufacturer) utilizing multiple measurements and a retrospective correction of the CEST spectra prior to evaluation, repeated for every image volume. The ideal case, however, would be a measurement with completely perfect B_0 homogeneity and unambiguously known water frequency. A method discussed in the literature is the previously mentioned WASSR, in which one acquires a correction dataset for repeated use. This alternative has been set aside in this dissertation but may provide a time saving solution when several image volumes are collected.

In order to increase SNR in the CEST images, a more prominent saturation effect should be established before the imaging block. Increased saturation pulse duration or number of pulses are straightforward alternatives as long as SAR limits are not overridden. Maximum CEST effect should be established with a total saturation time in the order of one T_1 and a repetition time that allow complete restoration of magnetization between blocks, but increased repetition time suffers from diminishing returns and complete restoration is not really necessary. Finally, it is also feasible to use parallel imaging to increase the number of saturation periods without suffering from unreasonably time consuming scans.

A vital lesson from the practical investigations with gagCEST is that some kind of reference measurement of CEST effect must be done. The need to carefully shim and adjust the measurement makes absolute quantification difficult. The simplest phantom with only CS-A in PBS was used to construct CEST spectra in MatLab, and the asymmetry analysis could be used to identify each of the vials, however only in relation to the other. So if *in vivo* measurements are to provide information about the absolute content of GAG, some external or internal reference phantom must be present in the scan.

Moreover, when comparing CEST signal in different tissue it is important to remember that the technique is inherently unspecific. All labile protons within the saturation band will be effected and the resulting signal may not only depend on the solute of interest. All sugar contains several hydroxyl groups similar to CS, however, not all exhibit chemical exchange. Agarose is an example of a macro molecule with a symmetric MT spectrum. The actual MT behavior for all proteins and fibers in the meniscus and cartilage is not known by the author.

Finally, more technical considerations and investigations can be found in the area of saturation pulse design. The Bloch equations for saturation of several spin pools are complex, and the effects of exchange on relaxation and the spillover of RF power introduce interesting perturbations in the models. There are many ways to analytically or by means of simulations investigate these issues.

6 References

1. Vincent TL, Watt FE (2010) Osteoarthritis. *Medicine* 38(3):151–156
2. Owman H, Tiderius CJ, Neuman P, Nyquist F, Dahlberg LE (2008) Association between findings on delayed gadolinium-enhanced magnetic resonance imaging of cartilage and future knee osteoarthritis. *Arthritis and rheumatism* 58(6):1727–30
3. Ling W, Regatte RR, Navon G, Jerschow A (2008) Assessment of glycosaminoglycan concentration in vivo by chemical exchange-dependent saturation transfer (gagCEST). *Proceedings of the National Academy of Sciences of the United States of America* 105(7):2266–70
4. Jellus V, Paul D, Lauer L (2011) Cartilage Quality Assessment by Using Glycosaminoglycan Chemical Exchange Saturation Transfer and ²³Na MR Imaging at 7 T. *Radiology* 260(1):257–264
5. Kim M, Chan Q, Anthony M-P, Cheung KMC, Samartzis D, Khong P-L (2011) Assessment of glycosaminoglycan distribution in human lumbar intervertebral discs using chemical exchange saturation transfer at 3 T: feasibility and initial experience. *NMR in biomedicine* 24(9):1137–1144
6. Kiani C, Chen L, Wu YJ, Yee AJ, Yang BB (2002) Structure and function of aggrecan. *Cell research* 12(1):19–32
7. Dudhia J (2005) Aggrecan, aging and assembly in articular cartilage. *Cellular and molecular life sciences* : CMLS 62(19-20):2241–56
8. Stubendorff JJ, Lammentausta E, Struglics A, Lindberg L, Heinegård D, Dahlberg LE (2012) Is cartilage sGAG content related to early changes in cartilage disease? Implications for interpretation of dGEMRIC. *Osteoarthritis and cartilage / OARS, Osteoarthritis Research Society* 20(5):396–404
9. Torshizy H, Gold G, Chung C, Angel MJ, Sgaglione NA, Sharon S (2008) Cartilage. In: Pedowitz R, Chung CB, Resnick D (eds) *Magnetic Resonance Imaging in Orthopedic Sports Medicine*. Springer, New York, pp 45–81

10. Goldring MB, Goldring SR (2007) Osteoarthritis. *Journal of Cellular Physiology* 213(3):626–634
11. Gore JC, Kennan RP (1999) Physical and Physiological basis of Magnetic Relaxation. In: Stark DD, Bradley WG (eds) *Magnetic Resonance Imaging Part 1*, 3rd ed. Mosby, Missouri, pp 33–43
12. Williamson MP (2006) The Nuclear Overhauser Effect. In: Webb GA (ed) *Modern Magnetic Resonance*, 2008 editi. Springer, Dordrecht, pp 409–412
13. Henkelman RM, Stanisz GJ, Graham SJ (2001) Magnetization transfer in MRI : a review. *NMR in Biomedicine* 14(2):57–64
14. Bain A (2003) Chemical exchange in NMR. *Progress in Nuclear Magnetic Resonance Spectroscopy* 43(3-4):63–103
15. Wolff S, Balaban R (1990) NMR imaging of labile proton exchange. *Journal of Magnetic Resonance* 86(1):164–169
16. Mcfarland EW, Neuringer LJ, Kushmerick MJ (1988) Chemical exchange magnetic resonance imaging (CHEMI). *Magnetic Resonance Imaging* 6(5):507–515
17. Singh A, Haris M, Cai K, Kasey VB, Kogan F, Reddy D, Hariharan H, Reddy R (2011) Chemical exchange saturation transfer magnetic resonance imaging of human knee cartilage at 3 T and 7 T. *Magnetic resonance in medicine : official journal of the Society of Magnetic Resonance in Medicine / Society of Magnetic Resonance in Medicine* 68(2):588–94
18. Kim M, Gillen J, Landman BA, Zhou J, van Zijl PCM (2009) Water saturation shift referencing (WASSR) for chemical exchange saturation transfer (CEST) experiments. *Magnetic resonance in medicine : official journal of the Society of Magnetic Resonance in Medicine / Society of Magnetic Resonance in Medicine* 61(6):1441–50
19. Zu Z, Li K, Janve V a, Does MD, Gochberg DF (2011) Optimizing pulsed-chemical exchange saturation transfer imaging sequences. *Magnetic resonance in medicine : official journal of the Society of Magnetic Resonance in Medicine / Society of Magnetic Resonance in Medicine* 66(4):1100–8
20. Zhou J, Wilson D a, Sun PZ, Klaus J a, Van Zijl PCM (2004) Quantitative description of proton exchange processes between water and endogenous and exogenous agents for WEX, CEST, and APT experiments. *Magnetic resonance in medicine : official journal of the Society of Magnetic Resonance in Medicine / Society of Magnetic Resonance in Medicine* 51(5):945–52
21. Schmitt B, Zaiss M, Zhou J, Bachert P (2011) Optimization of pulse train presaturation for CEST imaging in clinical scanners. *Magnetic resonance in medicine : official journal of the Society of Magnetic Resonance in Medicine / Society of Magnetic Resonance in Medicine* 65(6):1620–9
22. Sun PZ, van Zijl PCM, Zhou J (2005) Optimization of the irradiation power in chemical exchange dependent saturation transfer experiments. *Journal of magnetic resonance (San Diego, Calif : 1997)* 175(2):193–200
23. Sun PZ, Farrar CT, Sorensen AG (2007) Correction for artifacts induced by B(0) and B(1) field inhomogeneities in pH-sensitive chemical exchange saturation transfer (CEST) imaging.

- Magnetic resonance in medicine : official journal of the Society of Magnetic Resonance in Medicine / Society of Magnetic Resonance in Medicine 58(6):1207–15
24. Ling W, Regatte R, Schweitzer ME, Jerschow A (2008) Characterization of bovine patellar cartilage by NMR. *NMR in Biomedicine* 21(3):289–295
 25. Futsaeter N, Gramstad T (1980) Studies of hydrogen bonding—XXXI. NMR studies of solute—solute—solvent interaction. *Spectrochimica Acta Part A: Molecular Spectroscopy* 36(12):1083–1088
 26. Ling W, Regatte R, Jerschow A (2007) GAG Content via Chemical Exchange Saturation Transfer: Assessing OA. *Proceedings of the International Society for Magnetic Resonance* 15. p 3811
 27. Walker P, Lerski RA, Vre RM-D, Binet J, Yane F (1988) VI. Preparation of agarose gels as reference substances for NMR relaxation time measurement. *Magnetic resonance Imaging* 6(2):215–222
 28. Eckstein F, Ateshian G, Burgkart R, et al (2006) Proposal for a nomenclature for magnetic resonance imaging based measures of articular cartilage in osteoarthritis. *Osteoarthritis and cartilage / OARS, Osteoarthritis Research Society* 14(10):974–83
 29. Temple MM, Bae WC, Chen MQ, Lotz M, Amiel D, Coutts RD, Sah RL (2007) Age- and site-associated biomechanical weakening of human articular cartilage of the femoral condyle. *Osteoarthritis and cartilage / OARS, Osteoarthritis Research Society* 15(9):1042–52
 30. Kawamura S, Lotito K, Rodeo S (2003) Biomechanics and healing response of the meniscus. *Operative Techniques in Sports Medicine* 11(2):68–76
 31. Peters T, Smillie I (1971) Studies on chemical composition of menisci from the human knee-joint. *Proceedings of the Royal Society of Medicine* 64(3):1967–1968
 32. Wiener E, Pfirrmann C, Hodler J (2010) Spatial variation in T1 of healthy human articular cartilage of the knee joint. *The British journal of radiology* 83(990):476–85
 33. Sun PZ, Cheung JS, Wang E, Benner T, Sorensen a G (2011) Fast multislice pH-weighted chemical exchange saturation transfer (CEST) MRI with Unevenly segmented RF irradiation. *Magnetic resonance in medicine : official journal of the Society of Magnetic Resonance in Medicine / Society of Magnetic Resonance in Medicine* 65(2):588–94

7 Appendix

7.1 Investigation of ring artefacts in CEST-measurements

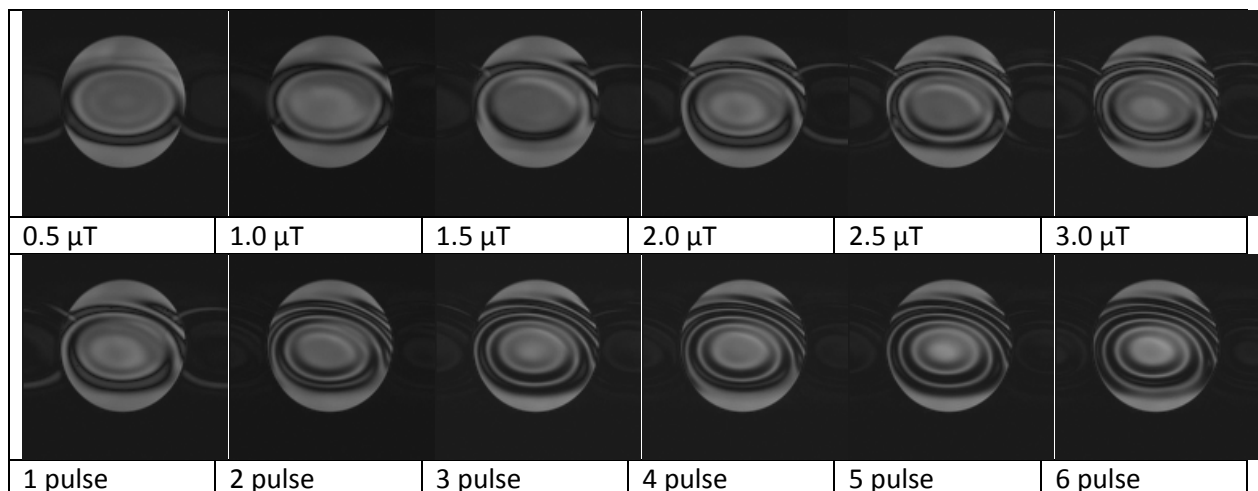
A minor side track investigation was performed to test if the ring artifacts observed in CEST images of water phantoms had anything to do with residual magnetization after saturation pulses. Contacts at Siemens described the phenomenon as residual magnetization, depending on saturation pulse design, phantom geometry and T2 relaxation – all three parameters were tested. The patterns occurring in the CEST image are the same that are visible in the saturated images. A CEST measurement is performed but only the images with saturation at .66 ppm (closest to 0 ppm saturation) are presented. One series with varied pulse power and one with varied number of pulses are presented.

Imaging parameters: 64 segments, TR 600, 128 resolution, TE 3.64, FA 11

Saturation parameters: Frequency offset 0,66 ppm, pulse length 99 ms, interpulse delay 99 ms, First series constant 1 pulse, second series constant 2.0 μT saturation power.

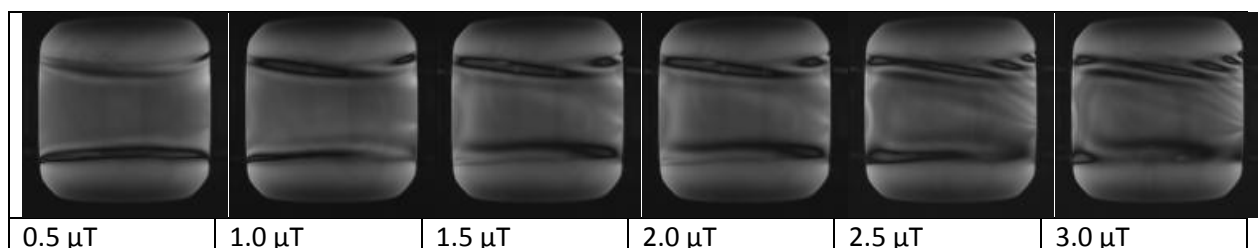
1 – Circular water phantom

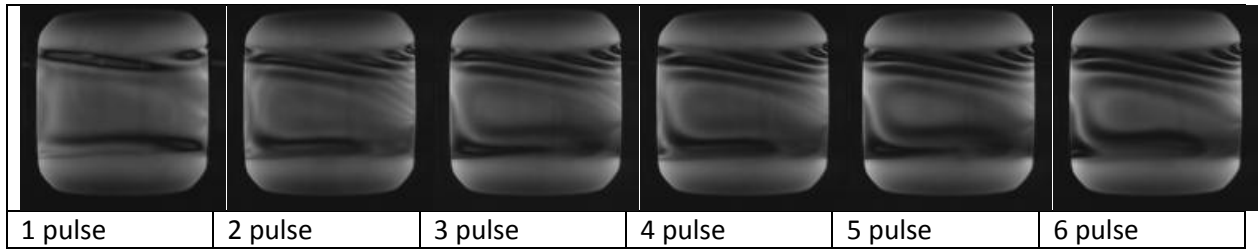
The circular phantom produce much artifacts. We see an increasing amplitude variation and number of the ring patterns with both increasing pulse strength and number of pulses.



2 – Almost square phantom

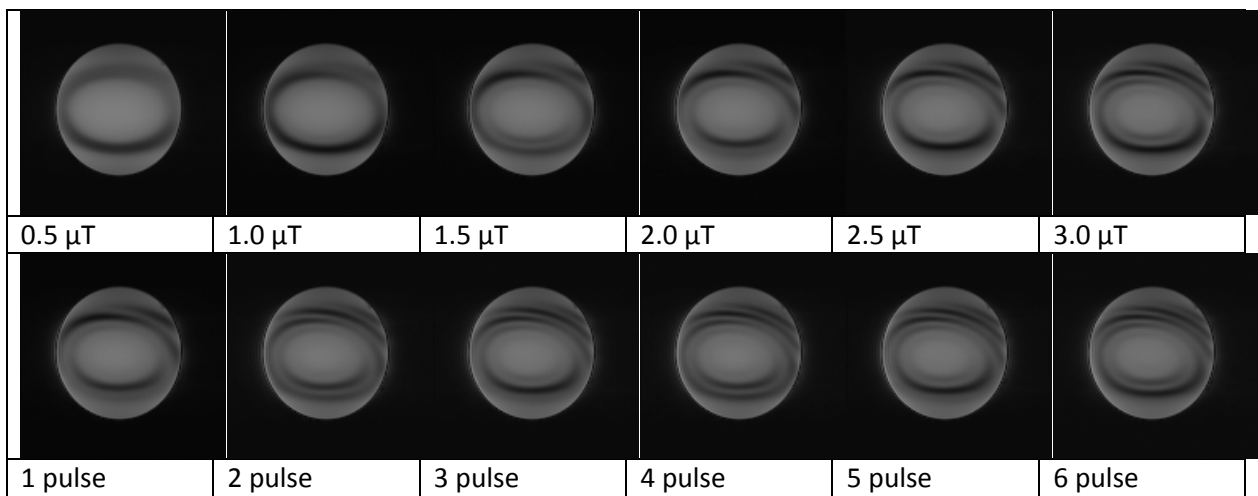
The severity of the artifacts is reduced and it is possible to conclude that the geometry of the object has a large effect on the patterns.





3 – Round phantom with 3 mM DOTAREM

With DOTAREM added to water the T2 relaxation time is decreased from ca 2500 ms to 100 ms and T1 from 3000 ms to 150 ms. The amplitude of the ring patterns is diminished as well as the number of rings we can observe. This is likely a combined effect of decreasing residual magnetization after the saturation pulses but also an overall increase in signal due to T1-relaxation. However, since centric encoding is used the T1 relaxation effect is likely to be less prominent.



Conclusion

The ring patterns can be observed in all measurements with the current saturation scheme. The ideal case would be completely homogeneous images at this stage, with a low signal due to homogeneously saturated spins. This however, is best achieved with long saturation pulse trains or continuous irradiation, which is impossible *in vivo* due to SAR limits.